Control Engineering Practice 71 (2018) 61–78

Contents lists available at ScienceDirect

Control Engineering Practice

journal homepage: www.elsevier.com/locate/conengprac

Robust fault detection with Interval Valued Uncertainties in Bond Graph Framework

Mayank-Shekhar Jha [a,*], Genevieve Dauphin-Tanguy [a], Belkacem Ould-Bouamama [b]

[a] CRIStAL UMR CNRS 9189, Ecole Centrale de Lille, Cité Scientifique 59650 Villeneuve d'Ascq, France
[b] CRIStAL UMR CNRS 9189, Polytech Lille, Université de Lille 1, Cité Scientifique 59650 Villeneuve d'Ascq, France

ARTICLE INFO

Keywords:
Bond graph
Analytical redundancy relations
Interval analysis
Uncertain system
Fault detection
Interval-valued uncertainties

ABSTRACT

This paper describes a novel formalism for modelling uncertain system parameters and measurements, as interval models in a Bond Graph (BG) modelling framework. The main scientific interest remains in integrating the benefits of BG modelling technique and properties of Interval Analysis (IA), for efficient diagnosis of uncertain systems. Structural properties of Bond graphs in Linear Fractional transformation (BG-LFT) are exploited to model interval-valued uncertainties over a BG model in order to form an uncertain BG. The inherent causal properties are exploited to generate interval-valued fault indicators. Then, various properties of IA are used to generate point valued residual and interval-valued thresholds. The latter must contain the point valued residuals under nominal system functioning. A systematic procedure is proposed for passive-type fault detection method which is robust to uncertain system parameters and measurements. The viability of the method is shown through experimental study of a steam generator system. The limitations associated with existing fault detection method based on BG-LFT are alleviated by the proposed approach. Moreover, it is shown that proposed approach generalizes the BG-LFT method. This work forms the initial step towards integrating interval analysis based capabilities in BG framework for fault detection and health monitoring of uncertain systems.

1. Introduction

Advanced methods of supervision, fault detection and fault diagnostics become increasingly significant for improving the reliability, safety and efficiency of technical processes in various domains of engineering (Chen & Patton, 2012; Gertler, 1997; Isermann, 2005; Samantaray & Bouamama, 2008). The past decade has seen tremendous usage of *Analytical Redundancy Relations* (ARRs) for the purpose of fault detection (FD) and isolation (FDI) (Ould Bouamama, Medjaher, Bayart, Samantaray, & Conrad, 2005; Staroswiecki & Comtet-Varga, 2001). ARRs represent the physical constraints laws derived from the mathematical model of the system. They have the form: $\boldsymbol{h}(\boldsymbol{k}) = 0$ for any function $\boldsymbol{h}$ and set of known variables $\boldsymbol{k}$. ARRs are usually sensitive to known system parameters (like resistor in an electrical circuit) and measurements (sensor data, control inputs etc.). Residuals are the numerical evaluation of ARRs. Ideally, residuals remain within a certain bound of error when evaluated using measured data from the real system (Chen & Patton, 2012).

Recently, the Bond Graph (BG) modelling technique has been used extensively for ARR based supervision (Karnopp, Margolis, & Rosenberg, 2012; Rosenberg & Karnopp, 1972). BG has been established as an efficient modelling tool due to its well-developed graphical, structural and causal properties. A concise discussion on BG technique is provided in Appendix A. For a detailed introduction from *ab-initio* (causal and structural properties), readers are referred to Borutzky (2011), Karnopp et al. (2012), Mukherjee and Samantaray (2006) and Thoma and Bouamama (2000). Traditionally, BG models in *preferred integral causality* have been used for simulations/analysis and *preferred derivative causality* has been exploited for development of FD theory and supervision. *Derivative causality* leads to alleviation of initial condition problems. BG enabled FD for deterministic systems and notion of monitorability, isolability, fault signature matrix, ARR generation algorithms etc. are well detailed in Medjaher, Samantaray, Ould Bouamama, and Staroswiecki (2006) and Ould Bouamama, Medjaher, Samantaray, and Staroswiecki (2006). Some of the major FD related works include supervision of thermo-chemical systems (Bouamama, Samantaray, Medjaher, Staroswiecki, & Dauphin-Tanguy, 2005; Bouamama, Staroswiecki, Riera, & Cherifi, 2000; Medjaher et al., 2006), industrial chemical reactors (El Harabi,

* Corresponding author.
E-mail addresses: mayank-shekhar.jha@univ-lorraine.fr (M.-S. Jha), genevieve.dauphin-tanguy@ec-lille.fr (G. Dauphin-Tanguy), Belkacem.Ouldbouamama@polytech-lille.fr (B. Ould-Bouamama).

https://doi.org/10.1016/j.conengprac.2017.10.009
Received 23 January 2017; Received in revised form 12 October 2017; Accepted 13 October 2017
0967-0661/

Nomenclature

Abbreviations

ARR	Analytical Redundancy Relations
BG	Bond Graph
BG-LFT	Bond Graph in Linear Fractional Transformation
FDI	Fault Detection and Isolation
FD	Fault Detection
IA	Interval Analysis
I-ARR	Interval-valued Analytical Redundancy Relations
IEF	Interval Extension Functions
N-IEF	Natural Interval Extension Function
RIF	Rational Interval Function
URIF	uncertain residual interval function

Notations

θ	System parameter
θ^d	System parameter under degradation (prognostic candidate)
θ_n	Nominal value of θ^d
$\Delta\theta$	Additive uncertainty on θ
δ_θ	Multiplicative uncertainty on θ
$[\delta_\theta]$	Multiplicative uncertainty in interval form, equivalent to $[\underline{\delta_\theta}, \overline{\delta_\theta}]$
$[w_\theta]$	Uncertain effort or flow brought by interval uncertainty on θ, to the system.
SSe (SSf)	Dualized source of effort (flow)
$[-\Delta SSe_l, \Delta SSe_u]$	Interval valued Uncertainty on SSe
$[\underline{R}, \overline{R}]$	Interval valued ARR (I-ARR)
$R_n(t)$	Nominal part of the I-ARR $[\underline{R}, \overline{R}]$
$r_n(t)$	Numerical evaluation of the nominal part $R_n(t)$ of I-ARR
Ψ	Function with point-valued nominal parameters as arguments
$\boldsymbol{\Psi}$	URIF or Interval function of Ψ with interval valued arguments
$[\underline{B(t)}, \overline{B(t)}]$	Range or interval evaluation of URIF $\boldsymbol{\Psi}$
MSe^*	Virtual source of effort
$[\zeta_{SSe}]$	Notation denoting $[-\Delta SSe_l, \Delta SSe_u]$

Ould-Bouamama, Gayed, & Abdelkrim, 2010) etc. A comprehensive review of BG based supervision is provided in Bouamama, Biswas, Loureiro, and Merzouki (2014) and Ould-Bouamama, El Harabi, Abdelkrim, and Ben Gayed (2012).

The last decade has witnessed a successful transition of BG based FD from deterministic domain to uncertain systems. This has been possible mainly due to emergence of BG in Linear Fractional Transformation (BG-LFT), for uncertain systems (Dauphin-Tanguy and Kam, 1999). BG-LFT methodology is well detailed in Sié Kam and Dauphin-Tanguy (2005). BG-LFT models represent parametric uncertainties in such a way that causal, structural and behavioural properties of BG theory remain applicable for successful FD. Robust FDI is achieved through generation of adaptive thresholds (*passive* type of diagnosis) which are robust to parametric uncertainties (Djeziri, Merzouki, Bouamama, and Dauphin-Tanguy, 2007). In Djeziri, Ould Bouamama, and Merzouki (2009b), BG-LFT model of an uncertain steam generator is used for robust FDI, (Djeziri, Merzouki, & Bouamama, 2009a) describes the robust monitoring of electric vehicle, (Niu, Zhao, Defoort, & Pecht, 2014) employs BG-LFT and auto-regressive kernel regression based threshold monitoring, (Benmoussa, Bouamama, & Merzouki, 2014; Loureiro, Benmoussa, Touati, Merzouki, & Ould Bouamama, 2014) deal with BG-LFT enabled robust FDI of intelligent vehicles and autonomous systems, (Touati, Merzouki, & Ould Bouamama, 2012) extends the methodology by including measurement uncertainties on BG-LFT. In this context, it is noteworthy to highlight that uncertain parameters may be broadly classified into two categories: (i) uncertain physical components (electrical resistances, capacitors, etc.) where uncertainty manifests in terms of manufacturing errors or tolerance-of-manufacturing (percentage errors) on either side of the fabricated value (nominal value), (ii) uncertain physical phenomena that deviate or exhibit natural variations based upon different operational conditions (friction coefficient, temperature dependent electrical resistivity etc.) and usually vary unidirectionally. Presence of uncertainties lead to the requirement of robustness. In the context of supervision, robust FD methods imply preferable sensitivity to faults/fault indicators and robustness against uncertainties, environmental noises etc.

In this context, although BG-LFT has been exploited for mitigation of uncertainty related issues, little efforts have been made to ameliorate the methodology itself. For instance, therein, parametric uncertainties are quantified in a statistical manner and uncertain parameters are modelled with equal magnitudes of additive (or multiplicative) uncertainties on either sides of its respective nominal value. As BG-LFT method is envisaged as a unified modelling language for various energetic systems, the existing method limits its scope in incorporating all types of uncertain components, viz., physical components and physical phenomena. Furthermore, it is noteworthy that efficiency of any *passive* type of FD significantly depends upon the sensitivity of the thresholds generated for detection of faults.

On the other hand, bounding approaches employ interval models to model the uncertain system variables and parameters etc., enabling variation of the interval variable within pre-defined numeric intervals (Moore, 1979). Interval Analysis (IA) deals with computations involving intervals defined as set of real numbers $\{x|\underline{x} \le x \le \bar{x}\}$ denoted as $X = \left[\underline{x}, \bar{x}\right]$, where $\underline{x}$ is the infimum and $\bar{x}$ is the supremum. The set of closed intervals is $I(\Re) = \{[a, b]\,|a, b \in \Re, a \le b\}$. Being extension to real numbers; a real number x can be treated as a *degenerate interval* $\left[x, x\right]$. Interval arithmetic generalizes real arithmetic. Appendix B lists important properties and definitions related to IA. Readers are referred to Moore (1979) and Moore, Kearfott, and Cloud (2009) for details of IA. Moreover, classical interval-arithmetic based FDI can be referred in Karim, Jauberthie, and Combacau (2008), Rinner and Weiss (2004).

Recently, Jha, Dauphin-Tanguy, and Ould Bouamama (2014b) proposed a strategy involving BG-LFT and IA, wherein the thresholds were generated by treating the uncertain part of BG-LFT derived ARR, as an *interval extension function* (IEF). In Jha, Dauphin-Tanguy, and Ould Bouamama (2014a), the latter was integrated in a health monitoring framework as a diagnostic module. However, these previous attempts did not discuss the interval propagation strategy and sought the description of a formalism that models various types of uncertainties (parametric and measurement) using BGs. Furthermore, in these works the method was neither applied in real time nor compared with existing methods.

This paper describes a novel formalism of modelling the uncertain system parameters and measurements, in interval form under BG framework. The main scientific interest remains in integrating the benefits of BG technique with IA properties leading to efficient diagnosis of uncertain systems. A systematic procedure is proposed for *passive* type fault detection, robust to uncertain system parameters and measurements. The proposed method alleviates several limitation associated with BG-LFT based FDI. Moreover, I-ARR generalizes the BG-LFT method technique through usage of interval models.

The paper is divided into 6 sections. After the introduction section, Section 2 introduces interval modelling technique in BG framework. Section 3 establishes the procedure to generate interval-valued fault indicators termed as Interval-Valued analytical redundancy relations (I-ARR). Further, properties of IA are used to generate point valued residual and interval-valued thresholds over the latter.

I-ARRs and discusses various aspects related to interval calculations and implementation. Section 4 presents the implementation of method on steam generator system. Section 5 presents a comparative study between the I-ARR method and the BG-LFT method. Section 6 draws conclusions.

2. Modelling uncertainties as interval models

In a BG framework, nominal model of a deterministic dynamical system may be modelled in preferred integral causality. Let system parameter vector be $\boldsymbol{\theta} \in \mathbb{R}^{N_\theta}$ which constitutes capacitance element vector $\boldsymbol{C}$, *inertial* element vector $\boldsymbol{I}$, *dissipation* element vector $\boldsymbol{R}$, *transformer* element vector $\boldsymbol{TY}$ and *gyrator* element vector $\boldsymbol{GY}$. The measurement sensor vector is formed by $\mathbf{Y}(t) \in [\boldsymbol{De}(t), \boldsymbol{Df}(t)]^T$ with $\boldsymbol{De}(t) \in \mathbb{R}^{N_{De}}$ being *effort sensor* vector and $\boldsymbol{Df}(t) \in \mathbb{R}^{N_{Df}}$ being the *flow sensor* vector. The control/input vector is formed by $\mathbf{U}(t) \in [\boldsymbol{Se}(t), \boldsymbol{Sf}(t)]^T$ with $\boldsymbol{Se}(t) \in \mathbb{R}^{N_{se}}$ and $\boldsymbol{Sf}(t) \in \mathbb{R}^{N_{Sf}}$ being respectively, the *source of effort* and *source of flow* vectors.

2.1. Parametric uncertainty

An uncertain system parameter θ, can be represented in interval form as,

$$\left[\underline{\theta}, \bar{\theta}\right] = \left[\theta_n - \Delta\theta_l, \theta_n + \Delta\theta_u\right] \tag{1}$$

where, $\underline{\theta} = \sup\{a \in \mathbb{R} \cup \{-\infty, \infty\} | \forall\theta \in \left[\underline{\theta}, \bar{\theta}\right], a \le \theta\}$ and $\bar{\theta} = \inf\{b \in \mathbb{R} \cup \{-\infty, \infty\} | \forall\theta \in \left[\underline{\theta}, \bar{\theta}\right], \theta \le b\}$ with *inf* and *sup* as the *infimum* and *supremum* operators respectively. $\Delta\theta_l$ and $\Delta\theta_u$ are the additive uncertainty/deviation on the left and right sides respectively, over the respective nominal value θ_n, such that $\Delta\theta_l \ge 0$ and $\Delta\theta_u \ge 0$. The parameter θ_n may be treated as a *degenerate interval* $\left[\theta_n, \theta_n\right]$, with equal magnitude of upper and lower bounds. This way, an uncertain parameter may be modelled as combination of its nominal interval value and uncertain additive interval as,

$$\left[\underline{\theta}, \bar{\theta}\right] = \left[\theta_n, \theta_n\right] + \left[-\Delta\theta_l, \Delta\theta_u\right] \tag{2}$$

The multiplicative form of representation of uncertainty is useful for accounting relative uncertainty/errors. The *multiplicative interval uncertainty* denoted $\left[\underline{\delta_\theta}, \overline{\delta_\theta}\right]$, may be obtained as in (3), where $\Delta\theta_l \ge 0, \Delta\theta_u \ge 0$.

$$\left[\underline{\delta_\theta}, \overline{\delta_\theta}\right] = \left[-\Delta\theta_l/\theta_n, \Delta\theta_u/\theta_n\right] \tag{3}$$

Then, (2) may equivalently be written as,

$$\left[\underline{\theta}, \bar{\theta}\right] = \theta_n.\left(1 + \left[\underline{\delta_\theta}, \overline{\delta_\theta}\right]\right) \tag{4}$$

If the constitutive law is written in terms of $\frac{1}{\theta}$, it may be expressed as,

$$\left[\frac{1}{\underline{\theta}}, \frac{1}{\bar{\theta}}\right] = \frac{1}{\left[\theta_n - \Delta\theta_l, \theta_n + \Delta\theta_u\right]} = \frac{1}{\theta_n}.\left(1 + \left[\underline{\delta_{1/\theta}}, \overline{\delta_{1/\theta}}\right]\right) \tag{5}$$

with $\theta_n \ne 0$; $0 \notin \left[\frac{1}{\underline{\theta}}, \frac{1}{\bar{\theta}}\right]$.

Value of $\left[\underline{\delta_{1/\theta}}, \overline{\delta_{1/\theta}}\right]$ is obtained from (5) by applying rules of Interval arithmetic (see Property B.2) as,

$$\begin{aligned}
\left[\underline{\delta_{1/\theta}}, \overline{\delta_{1/\theta}}\right] &= \frac{\theta_n}{\left[\theta_n - \Delta\theta_l, \theta_n + \Delta\theta_u\right]} - 1 \\
\left[\underline{\delta_{1/\theta}}, \overline{\delta_{1/\theta}}\right] &= \left[\frac{\theta_n}{\theta_n + \Delta\theta_u}, \frac{\theta_n}{\theta_n - \Delta\theta_l}\right] - 1 \\
\left[\underline{\delta_{1/\theta}}, \overline{\delta_{1/\theta}}\right] &= \left[\frac{-\Delta\theta_u}{\theta_n + \Delta\theta_u}, \frac{\Delta\theta_l}{\theta_n - \Delta\theta_l}\right]
\end{aligned} \tag{6}$$

2.1.1. Representation on bond graph

For any BG element $\theta \in \{\boldsymbol{R}, \boldsymbol{I}, \boldsymbol{C}, \boldsymbol{TF}, \boldsymbol{GY}\}$, the nominal parametric value (a degenerate interval) $\theta_n \in \{\boldsymbol{R_n}, \boldsymbol{I_n}, \boldsymbol{C_n}, \boldsymbol{TF_n}, \boldsymbol{GY_n}\}$ is decoupled from its uncertain interval part $[\delta_\theta]\theta_n \in \{[\delta_R]\boldsymbol{R_n}, [\delta_I]\boldsymbol{I_n}, [\delta_C]\boldsymbol{C_n}, [\delta_{TF}]\boldsymbol{TF_n}, [\delta_{GY}]\boldsymbol{GY_n}\}$ where, for notational simplicity, $\left[\underline{\delta_\theta}, \overline{\delta_\theta}\right] \cong [\delta_\theta]$. The uncertain flow ($f_i$) and effort ($e_i$), brought-in at a BG junction by interval uncertainty $\left[\delta_{\theta_i}\right]$, are represented using fictive efforts $MSe : [w_i]$ or fictive flow inputs $MSf : [w_i]$ respectively. The latter are modulated by $\left[\delta_{\theta_i}\right] * (\theta_{i,n}.e_i)$ and $\left[\delta_{\theta_i}\right] * (\theta_{i,n}.f_i)$ respectively. For a pedagogical illustration, a resistor element R is considered. *Nominal case* (see Fig. 1): The characteristic equation with parameter in nominal state (without any uncertainty) is expressed as,

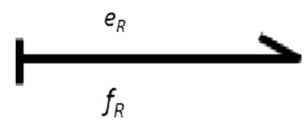

Fig. 1. Nominal R element (resistance causality).

$$e_R = \phi_R = R.f_R \tag{7}$$

Here, ϕ_θ denotes the constitutive equation of parameter θ.

Uncertain case. In *resistance* (imposed flow) causality (see Fig. 2): With multiplicative interval uncertainty $\left[\underline{\delta_R}, \overline{\delta_R}\right]$, the characteristic law is expressed as,

$$\begin{aligned}
\left[\underline{e_R}, \overline{e_R}\right] &= \left[\underline{R}, \overline{R}\right].f_R = R_n\left(1 + \left[\underline{\delta_R}, \overline{\delta_R}\right]\right).f_R \\
\left[\underline{e_R}, \overline{e_R}\right] &= \underbrace{\left[R_n, R_n\right].f_R}_{e_{R_n}} + \underbrace{\left(\left[\underline{\delta_R}, \overline{\delta_R}\right].R_n\right).f_R}_{e_{R_{unc}}}
\end{aligned} \tag{8}$$

$$\left[\underline{e_R}, \overline{e_R}\right] = \underbrace{\left[R_n, R_n\right].f_R}_{e_{R_n}} - \underbrace{\left[w_R\right]}_{-e_{R_{unc}}} \tag{9}$$

where $\left[w_R\right] = -\left[\underline{\delta_R}, \overline{\delta_R}\right].z_R = -\left[\underline{\delta_R}, \overline{\delta_R}\right].R_n.f_R$.

Clearly, the interval-valued uncertain effort $e_{R_{unc}}$ is brought at the 1-*junction* by $\left[w_R\right]$. Moreover, it is modulated by $-\left[\underline{\delta_R}, \overline{\delta_R}\right].R_n.f_R$.

Similarly, in *conductance* (imposed effort) causality (see Fig. 3), uncertain interval form $\left[\frac{1}{\underline{R}}, \frac{1}{\overline{R}}\right]$ can be expressed with the help of multiplicative uncertainty interval $\left[\underline{\delta_{1/R}}, \overline{\delta_{1/R}}\right]$ (c.f. (5), (6)) as, $\left[\underline{\delta_{1/R}}, \overline{\delta_{1/R}}\right] = \left[\frac{-\Delta R_u}{R_n + \Delta R_u}, \frac{\Delta R_l}{R_n - \Delta R_l}\right]$. The characteristic law $f_R = \frac{e_R}{R}$ can be expressed using uncertain interval form as,

$$\begin{aligned}
\left[\underline{f_R}, \overline{f_R}\right] &= \left[\frac{1}{\underline{R}}, \frac{1}{\overline{R}}\right].e_R = \frac{1}{R_n}.\left(1 + \left[\underline{\delta_{1/R}}, \overline{\delta_{1/R}}\right]\right).e_R \\
\left[\underline{f_R}, \overline{f_R}\right] &= \underbrace{\frac{e_R}{R_n}}_{f_{R_n}} + \underbrace{\left(\left[\underline{\delta_{1/R}}, \overline{\delta_{1/R}}\right].\left(1/R_n\right).e_R\right)}_{f_{R_{unc}}}
\end{aligned} \tag{10}$$

$$\left[\underline{f_R}, \overline{f_R}\right] = \frac{e_R}{R_n} - \underbrace{\left[w_{1/R}\right]}_{-f_{R_{unc}}} \tag{11}$$

where the interval-valued fictive input $\left[w_{1/R}\right] = -\left[\underline{\delta_{1/R}}, \overline{\delta_{1/R}}\right].z_{1/R} = -\left[\underline{\delta_{1/R}}, \overline{\delta_{1/R}}\right].\left(1/R_n\right).e_R$.

Remark. The negative sign added to the uncertain interval block and effort/flow bonds (see Fig. 2 and Fig. 3, comes from the power balance convention which is obeyed at 1-*junction* and 0-*junction* respectively. The virtual detectors De^* (Df^*) are used to represent the information exchange/transfer. A star '*' is added as a super-script for distinguishing the fictitious detectors (signals) from the real ones.

Interval uncertainty can be modelled and represented over other uncertain BG elements $\boldsymbol{I}, \boldsymbol{C}, \boldsymbol{GY}, \boldsymbol{TF}, \boldsymbol{RS}$ etc., using the established LFT form Sié Kam and Dauphin-Tanguy (2005).

A pedagogical example is considered for illustration.

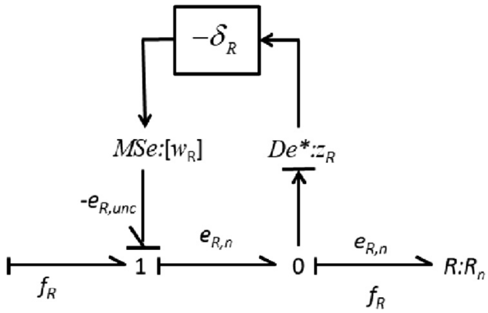

Fig. 2. Uncertain R element (resistance causality) in interval form.

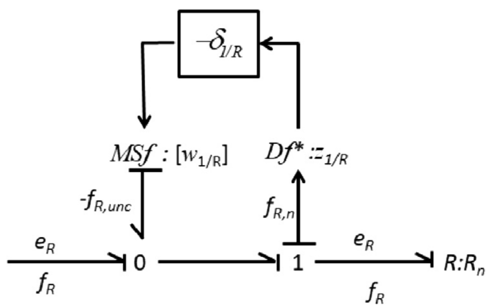

Fig. 3. Uncertain R element (resistance causality) in interval form.

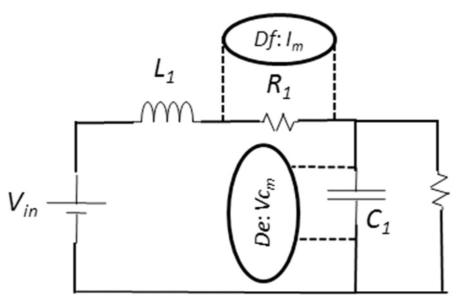

Fig. 4. $R{-}L{-}C$ electrical circuit for pedagogical illustration.

Example 1. Consider a pedagogical $R{-}L{-}C$ electrical circuit as shown in Fig. 4. The circuit current i through resistor R_1, inductor L_1 and capacitor C_1, and voltage across the capacitor are measured as I_m and Vc_m respectively. All of the system parameters and system measurements respectively, viz.: R_1, L_1, C_1, R_2, and De: Vc_m, Df: I_m ., are considered uncertain in nature. It should be noted that nominal effort Vc_m (flow I_m) sensors are represented using De (Df) elements.

Fig. 5 shows the nominal BG model (model with nominal parameters) of the electrical circuit in *preferred integral* causality (used for simulations, analysis). As discussed earlier, BG models in *preferred derivative causality* felicitate efficient diagnosis, as ARRs can be obtained preferably without initial conditions. The nominal BG model in *preferred derivative causality* is shown in Fig. 6. Therein, the sensors have been dualized to corresponding sources (supplying measured signal at junction) viz., $Df:I_m \rightarrow SSf:I_m$ and $De:Vc_m \rightarrow SSe:Vc_m$.

Once the diagnosis oriented BG has been obtained in Fig. 6, an uncertain BG can be constructed by representing each of the uncertain parameters over the nominal BG. The uncertain BG is shown in Fig. 7, with parametric uncertainty in interval form as discussed in this section.

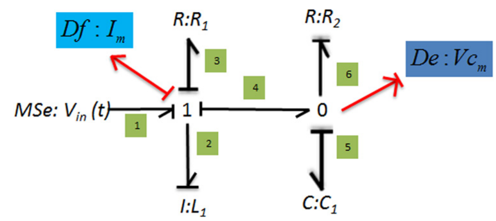

Fig. 5. BG model of the nominal electrical system in *preferred integral causality* (used mainly for simulations)

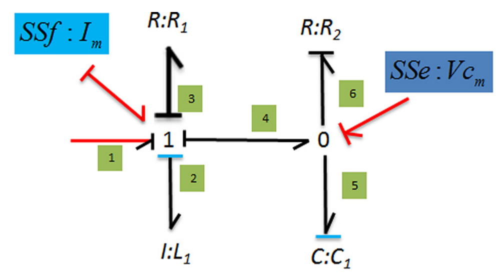

Fig. 6. BG model of the nominal electrical system in *preferred derivative causality* (used mainly for diagnosis)

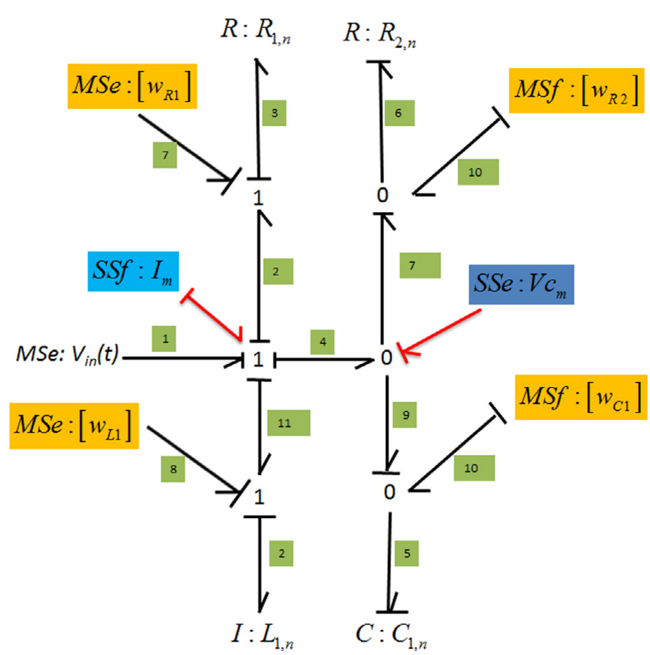

Fig. 7. Uncertain BG model of electrical system considered in Example 1, with only parametric uncertainties in interval form.

2.2. Measurement uncertainty

Measurement uncertainties can manifest in various forms, viz.: sensor drifts and associated limits, measurement bias, measurement errors, sensor tolerance limits etc. Similar to the previous section, measurement uncertainties can also be modelled in interval form. To that end, consider measurements of a signal Sn, such that its true measurement value Sn_t is not observable explicitly or remains hidden (unknown). The observed (known) measurement Sn_m is assumed to be uncertain in nature. The associated uncertainty is considered additive; it can be modelled in interval form as $[-\Delta Sn_l, \Delta Sn_u]$. Then, the true measurement value can be considered to be implicitly related to the

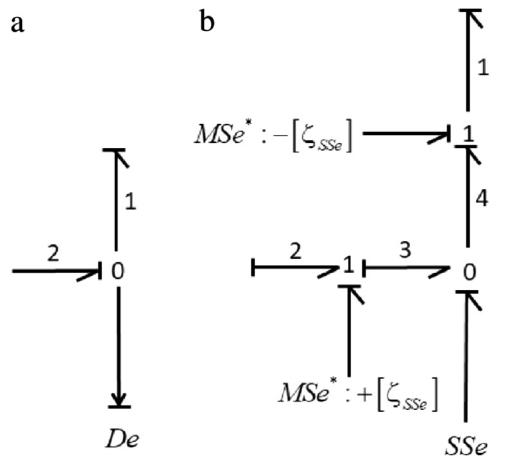

Fig. 8. Effort measurement, (a) Nominal BG (b) Dualized effort detector with measurement uncertainty in interval form on uncertain BG.

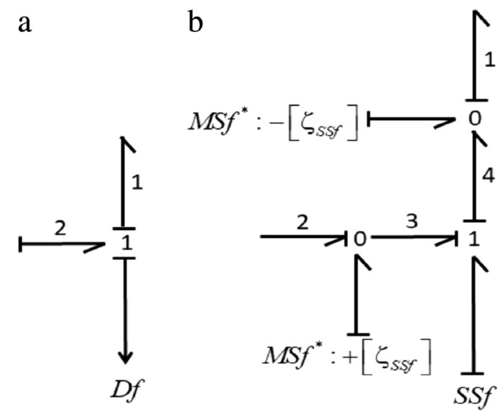

Fig. 9. Flow measurement, (a) Nominal BG (b) Dualized Flow detector with measurement uncertainty in interval form on uncertain BG.

observed measurement as,

$$\left[\underline{Sn_m}, \overline{Sn_m}\right] = Sn_t + \left[-\Delta Sn_l, \Delta Sn_u\right] \tag{12}$$

Thus, the true measurement value Sn_t can be obtained in interval form as,

$$\left[\underline{Sn_t}, \overline{Sn_t}\right] = \left[\underline{Sn_m}, \overline{Sn_m}\right] - \left[-\Delta Sn_l, \Delta Sn_u\right] \tag{13}$$

where ΔSn_l and ΔSn_u are respectively, the lower and upper interval bounds of the measurement uncertainty.

In BG framework, the measured signal Sn_m can manifest in form of *effort* (*flow*) signals, represented by *effort detector* (*flow detector*) De (Df) as shown in Fig. 8(a) and Fig. 9(a).

Further, the concept of detector *dualization* (Samantaray, Medjaher, Ould Bouamama, Staroswiecki, & Dauphin-Tanguy, 2006) is recalled for representation of (13) on an uncertain BG. Upon *dualization, effort detector* De (flow detector Df) becomes a *source of effort* SSe (*source of flow* SSf) and imposes only the *effort* (*flow*) signal at the 0-*junction* (1-*junction*) connected to the detector; as such, *flow* (*effort*) associated with SSe (SSf) is zero.

It should be noted that, measurement signal imposed by SSe (SSf) on the junction **0** (**1**) is a measured signal information. As such, all the bonds connected directly to the junction element **0** (**1**), carry the same measured *effort* (*flow*) information.

2.2.1. Uncertain effort measurement

Dualized effort detector (carrying measured signal) can be considered as $\left[\underline{SSe}, \overline{SSe}\right]_{measure} = \left[\underline{SSe_t}, \overline{SSe_t}\right]_{true} + \left[-\Delta SSe_l, \Delta SSe_u\right]$. The uncertainty interval is modelled by **virtual source** (fictitious) of effort $MSe^* : \left[-\Delta SSe_l, \Delta SSe_u\right]$. For notational simplicity, $MSe^* : \left[-\Delta SSe_l, \Delta SSe_u\right]$ is denoted as $MSe^* : \left[\zeta_{SSe}\right]$. Then, the true value of measurement as obtained in (13), can be represented on BG model as shown in Fig. 8. As the **0** *junction* in Fig. 8 is effort conservative; following equations can be derived from Fig. 8:

$$\begin{aligned}
\left[\underline{e_1}, \overline{e_1}\right]_{true} &= \left[e_4, e_4\right]_{measured} - \left[-\Delta SSe_l, \Delta SSe_u\right] \\
&= SSe + MSe^* : \left(-\left[-\Delta SSe_l, \Delta SSe_u\right]\right) \\
\left[\underline{e_2}, \overline{e_2}\right]_{true} &= \left[e_3, e_3\right]_{measured} - \left[-\Delta SSe_l, \Delta SSe_u\right] \\
&= SSe - MSe^* : \left(\left[-\Delta SSe_l, \Delta SSe_u\right]\right)
\end{aligned} \tag{14}$$

2.2.2. Uncertain flow measurement

A uncertain flow detector can be considered as $\left[\underline{SSf}, \overline{SSf}\right]_{measure} = \left[\underline{SSf_t}, \overline{SSf_t}\right]_{true} + \left[-\Delta SSf_l, \Delta SSf_u\right]$. The uncertainty interval is modelled by **virtual source** of flow $MSf^* : \left[-\Delta SSf_l, \Delta SSf_u\right]$ (denoted as $MSf^* : \left[\zeta_{SSf}\right]$). Then, the true value of measurement obtained in (13), can be represented on BG model shown in Fig. 9. As the **1** *junction* in Fig. 9 is flow conservative, following equations can be derived from Fig. 9:

$$\begin{aligned}
\left[\underline{f_1}, \overline{f_1}\right]_{true} &= \left[f_4, f_4\right]_{measured} - \left[-\Delta SSf_l, \Delta SSf_u\right] \\
&= SSf + MSf^* : \left(-\left[-\Delta SSf_l, \Delta SSf_u\right]\right) \\
\left[\underline{f_2}, \overline{f_2}\right]_{true} &= \left[f_3, f_3\right]_{measured} - \left[-\Delta SSf_l, \Delta SSf_u\right] \\
&= SSf - MSf^* : \left(\left[-\Delta SSf_l, \Delta SSf_u\right]\right)
\end{aligned} \tag{15}$$

Moreover, the representation of (13) for SSe and SSf can be achieved on uncertain BG for both kinds of bond orientations i.e. inward power orientation with respect to the junction (bond 2 in Fig. 8(a) and Fig. 9(a)) and outward power orientation with respect to the junction (bond 1 in Fig. 8(a) and Fig. 9(a)).

Example 1.1. Here, the RLC circuit presented in Example 1 is continued to include measurement uncertainties over the uncertain BG. The uncertain BG model with measurement uncertainties is shown in Fig. 10.

3. Robust fault detection

The causal and structural properties of a BG model are not altered due to introduction of uncertainties in LFT form over nominal BG (Djeziri, Merzouki, et al., 2009; Djeziri, Ould Bouamama, et al., 2009) as such, they remain unaffected when uncertainties are introduced in interval form on a nominal BG. It is assumed that the system is monitorable and observable. Moreover, the initial condition problem is avoided by adequate sensor placement. Considered uncertain parameter vector as $\left[\underline{\theta}, \overline{\theta}\right] \in \mathbb{R}^{N_m}$ where $N_m \leq N_\theta$, uncertain dualized effort detector vector as $\left[\underline{\mathbf{SSe}}, \overline{\mathbf{SSe}}\right] \in \mathbb{R}^{N_{Sse}}$ ($N_{SSe} \leq N_{De}$) and uncertain dualized flow detector vector as $\left[\underline{\mathbf{SSf}}, \overline{\mathbf{SSf}}\right] \in \mathbb{R}^{N_{Ssf}}$ ($N_{SSf} \leq N_{Df}$).

3.1. Interval-valued analytical redundancy relations

The ARR generation procedure for deterministic systems (Bouamama, Samantaray, Staroswiecki, & Dauphin-Tanguy, 2003) is a well-established method comprising of systematic rules for ARR derivation that consider aspects such as quantity and placement of sensors in the system for ARR derivation (Samantaray & Bouamama, 2008). Moreover, a systematic (programmable) and automatic procedure for ARR generation from BG models has been implemented in SYMBOL SHAKTI software (Mukherjee & Samantaray, 2005) which eases the process of ARR derivation and also leads to automated diagnostic steps.

Here, ARR generation strategy is adapted for BG model with interval-valued parameters and sensor measurements. This leads to generation of Interval-valued Analytical Redundancy Relations (I-ARRs). The I-ARRs are produced by energetic assessment at the junctions (0 and 1) of BG which are detectable i.e. connected to at least one detector (effort or flow).

The following steps are taken to generate I-ARRs:

Step 1: Preferred derivative causality is assigned to the nominal model and detectors De (Df) are dualized to SSe (SSf), wherever possible (see Fig. 6 with BG model in *preferred derivative causality* with dualized sensors, vis-à-vis Example 1).

Step 2: Parametric uncertainties and measurement uncertainties are modelled in interval form and represented on the nominal BG, to obtain the corresponding uncertain BG (see Fig. 10 for uncertain BG model of the electrical system in *Example* 1).

Step 3: The candidate ARRs are generated from "1" or "0" junction, where power conservation equation dictates that sum of efforts or flows, respectively, is equal to zero, as:

- for *0-junction*:

$$\sum s.\left[\underline{f},\overline{f}\right]+\sum Sf+\sum_{i=0}^{i\leq N_m} s_i.MSf\,:\,\left[w_i\right]=0 \tag{16}$$

- for *1*-junction:

$$\sum s.\left[\underline{e},\bar{e}\right]+\sum Se+\sum_{i=0}^{i\leq N_m} s_i.MSe\,:\,\left[w_i\right]=0 \tag{17}$$

with s being the sign rendered to a *bond* to respect energy convention. The unknown effort or flow variables are eliminated using *covering causal paths* from unknown variables to known (measured) variables (dualized detectors).

This generates I-ARRs $\left[\underline{R},\overline{R}\right]$ containing only known variables, as:

$$\left[\underline{R(t)},\overline{R(t)}\right]\,:\,\Xi\left(\begin{array}{l}\theta_n,\left[\underline{\theta},\bar{\theta}\right],\left[w_i\right],\left[\zeta_{\mathrm{SSe}}\right],\left[\zeta_{\mathrm{SSf}}\right],\\ \sum Se,\sum Sf,\mathbf{SSe}(t),\mathbf{SSf}(t)\end{array}\right) \tag{18}$$

where, Ξ is any non-linear function with point-valued and interval-valued arguments.

The I-ARR has two distinct parts (see (19)), viz., nominal part $R_n(t)$ and interval-valued part $\left[\underline{B(t)},\overline{B(t)}\right]$:

$$\left[\underline{R(t)},\overline{R(t)}\right]\,:\,R_n(t)+\left[\underline{B(t)},\overline{B(t)}\right] \tag{19}$$

As shown in (20), the *nominal part* is characterized by point valued function Ψ, sensitive to point valued nominal parameters; the latter serve as coefficients of point valued measurement variables. Interval-valued part $\left[\underline{B(t)},\overline{B(t)}\right]$ is identified as interval function $\boldsymbol{\Psi}$ which is sensitive to interval arguments in form of interval-valued uncertainties, as shown in (21).

$$R_n(t)=\Psi\left(\theta_{\mathrm{n}},\mathbf{SSe}(t),\mathbf{SSf}(t),\sum Se,\sum Sf\right) \tag{20}$$

$$\left[\underline{B(t)},\overline{B(t)}\right]=\boldsymbol{\Psi}\left(\left[\underline{\theta},\bar{\theta}\right],\left[\underline{\delta_\theta},\overline{\delta_\theta}\right],\left[\zeta_{\mathrm{SSe}}\right],\left[\zeta_{\mathrm{SSf}}\right],\mathbf{SSe}(t),\mathbf{SSf}(t)\right) \tag{21}$$

Here, $\left[\zeta_{SSe_i}\right]$ and $\left[\zeta_{SSf_i}\right]$ are respectively, the simplified notations (c.f. (14), (15)), for every $\left[\underline{SSe},\overline{SSe}\right]\in\left[\underline{\mathbf{SSe}},\overline{\mathbf{SSe}}\right]$ and $\left[\underline{SSf},\overline{SSf}\right]\in\left[\underline{\mathbf{SSf}},\overline{\mathbf{SSf}}\right]$.

The numerical evaluation of nominal part $R_n(t)$ is termed as *nominal residual* r_n, i.e. $r_n=\mathrm{eval}(R_n)$.

Moreover, $\boldsymbol{\Psi}$ being the interval-valued extension function of Ψ, is termed as *uncertain residual interval function* (URIF).

Also, $\left[\underline{B(t)},\overline{B(t)}\right]$ is the interval that represents the numerical evaluation of URIF $\boldsymbol{\Psi}$.

Example 1.3. Consider Example 1.1 and the uncertain BG shown in Fig. 10, to generate I-ARR from junction $\mathbf{1_1}$. To that end, causal path 1 (see Fig. 10) is covered starting from SSf: I_{m}. The schematic illustration of causal path is shown in Fig. 11.

This leads to derivation of I-ARR: $\left[\underline{R_{e1}},\overline{R_{e2}}\right]$ which is an interval function.

$$\begin{aligned}\left[\underline{R_{e1}},\overline{R_{e2}}\right]=&\;V_{in}(t)-\left(R_{1,n}+\left[\underline{\delta_{R_1}},\overline{\delta_{R_1}}\right]R_{1,n}\right)\\ &\times\left(SSf\,:\,I_m-MSf^*\,:\,\left(\left[-\Delta I_m,\Delta I_m\right]\right)\right)\\ &-\left(L_{1,n}+\left[\underline{\delta_{L_1}},\overline{\delta_{L_1}}\right]L_{1,n}\right)\\ &\times\frac{d\left(SSf\,:\,I_m-MSf^*\,:\,\left(\left[-\Delta I_m,\Delta I_m\right]\right)\right)}{dt}\\ &-\left(SSe\,:\,Vc_m-MSf^*\,:\,\left(\left[-\Delta Vc_m,\Delta Vc_m\right]\right)\right)\end{aligned} \tag{22}$$

This I-ARR can be easily decomposed into a point valued nominal residual $R_{e1,n}$ and interval-valued URIF $\left[\underline{B_{e1}(t)},\overline{B_{e1}(t)}\right]$, as:

$$\left[\underline{R_{e1}},\overline{R_{e2}}\right]=R_{e1,n}+\left[\underline{B_{e1}(t)},\overline{B_{e1}(t)}\right] \tag{23}$$

$$R_{e1,n}=V_{in}(t)-R_{1,n}I_m-L_{1,n}\frac{d\left(I_m\right)}{dt}-SSe\,:\,Vc_m$$

$$\begin{aligned}\left[\underline{B_{e1}(t)},\overline{B_{e1}(t)}\right]=&\;R_{1,n}\left[-\Delta I_m,\Delta I_m\right]-\left[\underline{\delta_{R_1}},\overline{\delta_{R_1}}\right]R_{1,n}.I_m+\left[\underline{\delta_{R_1}},\overline{\delta_{R_1}}\right]\\ &\times R_{1,n}\left[-\Delta I_m,\Delta I_m\right]+L_{1,n}\frac{d\left[-\Delta I_m,\Delta I_m\right]}{dt}\\ &+\left[\underline{\delta_{L_1}},\overline{\delta_{L_1}}\right]L_{1,n}\frac{d\left[-\Delta I_m,\Delta I_m\right]}{dt}-\left[\underline{\delta_{L_1}},\overline{\delta_{L_1}}\right]L_{1,n}\frac{d\left(I_m\right)}{dt}\\ &+\left[-\Delta Vc_m,\Delta Vc_m\right]\quad\square\end{aligned}$$

Remark. When the characteristic equation of any BG element(s) is such that *nominal residual* and URIF cannot be perfectly decoupled (nominal parameter(s) remains sensitive to interval-valued measurement variables), notion of interval *midpoint* (see Definition B.1) and interval *width* (see Definition B.2) are exploited to split the interval(s) into two parts consisting of point valued data and interval-valued data (see Property B.1).

3.2. Interval-valued Robust thresholds

Definition B.4 (Moore et al., 2009)**.** *Natural interval extension function* (N-IEF) F, of f is obtained, by replacing the real arguments with interval arguments and real operators (arithmetic etc.) by their equivalent interval operators, in the syntactic expression of the real function f.

Proposition 1. *The URIF $\boldsymbol{\Psi}$ can be considered as Natural Interval Extension Function (N-IEF) of Ψ .*

Proof. Consider a function Ψ which represents the nominal residual with point valued arguments, as

$$\Psi\left(\boldsymbol{\theta},\boldsymbol{\delta_\theta},\boldsymbol{\theta_n},\mathbf{SSe}(t),\mathbf{SSf}(t),\boldsymbol{\Delta SSe},\boldsymbol{\Delta SSe}\right) \tag{24}$$

where, $\forall\boldsymbol{x}$ such that $\boldsymbol{x}\in\arg(\Psi)$, $\exists\left[\underline{\boldsymbol{X}},\overline{\boldsymbol{X}}\right]$: $\boldsymbol{x}\in\left[\underline{\boldsymbol{X}},\overline{\boldsymbol{X}}\right]$. A corresponding interval-valued function URIF $\boldsymbol{\Psi}([\underline{\theta},\bar{\theta}],[\underline{\delta_\theta},\overline{\delta_\theta}],\theta_n,[\zeta_{\mathrm{SSe}}],[\zeta_{\mathrm{SSf}}],\mathbf{SSe}(t),\mathbf{SSf}(t))$, can be obtained by replacing the point valued arguments and arithmetic operators by the corresponding interval arguments and interval arithmetic operators respectively, in the syntactic expression of Ψ.

Definition B.6 (Moore et al., 2009)**.** A *rational interval function* (RIF) is an interval-valued function whose values are defined by a specific finite sequence of interval arithmetic operations.

Example 2. For any $x_1\in X_1,x_2\in X_2,x_3\in X_3$, function p defined as $p(x_1,x_2,x_3)=x_1e^{x_1-x_2^3+x_3^2}+x_2^3$. The corresponding interval extension $P(X_1,X_2,X_3)=X_1e^{X_1-X_2^3+X_3^2}+X_2^3$ can be computed through a finite sequences of interval arithmetic (evaluated as class code during

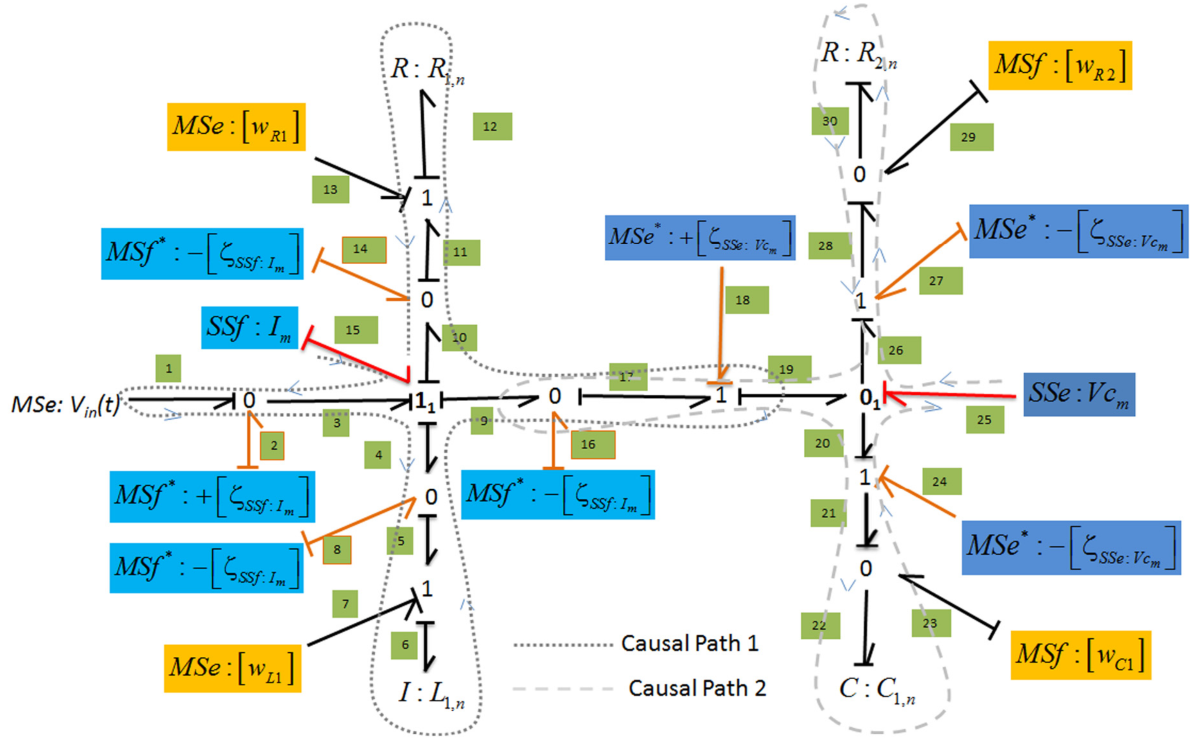

Fig. 10. Uncertain BG considered in Example 1 with parametric and measurement uncertianties in interval form.

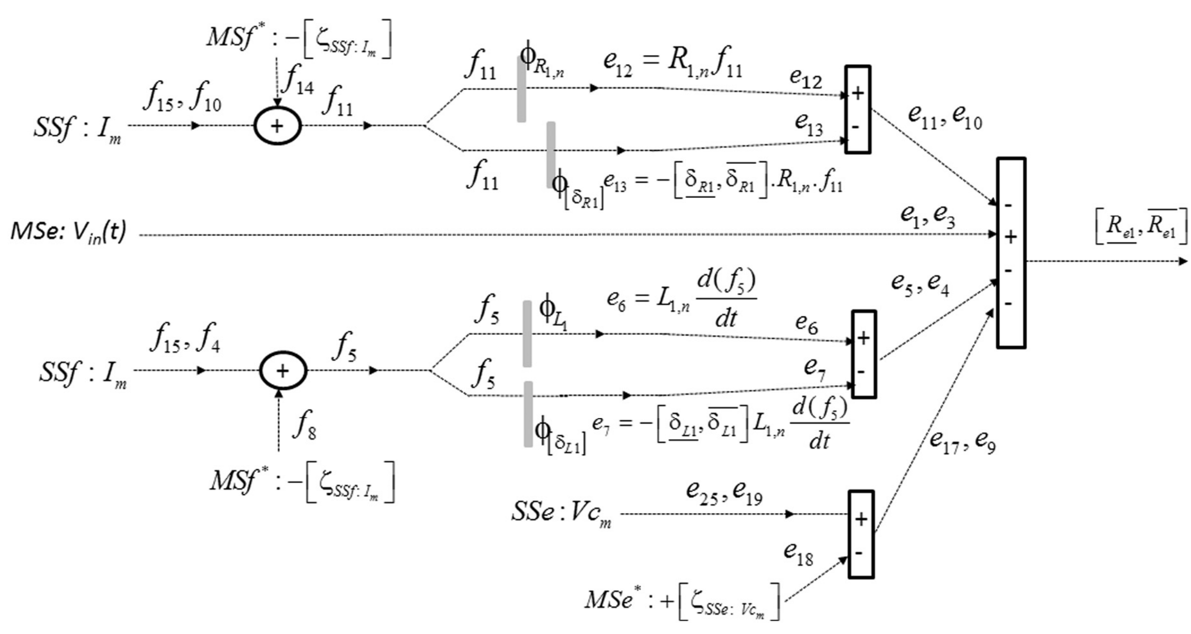

Fig. 11. Schematic illustration of covering causal path for I-ARR derivation at Junction 1_1 (see Fig. 10)

implementation (Moore et al., 2009), in order) as $P(X_1, X_2, X_3) : T_1 = X_2^3, T_2 = X_1 - T_1, T_3 = T_2 + X_3^2, T_4 = e^{T_3}, T_5 = X_1.T_4, T_5 + T_1$. Then, P is a rational interval function.

Proposition 2. *If $\boldsymbol{\Psi}$ is expressed as finite sequence of interval arithmetic operations, it can be considered as Rational Interval Function (RIF) of $\boldsymbol{\Psi}$.*

Proof. The proof follows definition of a RIF from above.

Proposition 3. *For any point valued vectors $\boldsymbol{\theta}, \boldsymbol{\delta_\theta}, \boldsymbol{\theta_n}, \mathbf{SSe}(t), \mathbf{SSf}(t), \boldsymbol{\Delta}\mathbf{SSe}$, $\boldsymbol{\Delta}\mathbf{SSe}$, bounded by interval limits $\boldsymbol{\Delta}\mathbf{SSe} \in \left[-\boldsymbol{\Delta}\mathbf{SSe_l}, \boldsymbol{\Delta}\mathbf{SSe_u}\right], \boldsymbol{\Delta}\mathbf{SSf} \in \left[-\boldsymbol{\Delta}\mathbf{SSf_l}, \boldsymbol{\Delta}\mathbf{SSf_u}\right], \theta \in \left[\underline{\theta}, \overline{\theta}\right], \delta_\theta \in \left[\underline{\delta_\theta}, \overline{\delta_\theta}\right]$; such that Uncertain Residual Interval Function (URIF) is expressed as finite sequence of interval arithmetic operations, range of URIF guarantees the containment of point valued nominal residual magnitude.*

Proof. From Property B.3, and Lemma B.4 (see Appendix B), $\boldsymbol{\Psi}$ can be regarded as an inclusion-isotonic function.

Then, from Theorem B.1 (see Appendix B), following can be guaranteed,

$$\boldsymbol{\Psi}\left(\delta_\theta, \boldsymbol{\Delta\theta}, \boldsymbol{\Delta SSe}, \boldsymbol{\Delta SSe}\right) \subseteq \boldsymbol{\Psi}\left(\begin{array}{c}\left[\underline{\theta}, \overline{\theta}\right], \left[\underline{\delta_\theta}, \overline{\delta_\theta}\right], \theta_n, \left[\zeta_{\mathbf{SSe}}\right], \left[\zeta_{\mathbf{SSf}}\right], \\ \mathbf{SSe}(t), \mathbf{SSf}(t)\end{array}\right) \quad (25)$$

where, $\forall \boldsymbol{x} : \boldsymbol{x} \in \arg(\Psi)$, $\exists \left[\underline{\boldsymbol{X}}, \overline{\boldsymbol{X}}\right] \in \arg(\boldsymbol{\Psi}) | \boldsymbol{x} \in \left[\underline{\boldsymbol{X}}, \overline{\boldsymbol{X}}\right]$.

Let $b(t)$ be defined as the numerical evaluation of $\Psi(\delta_\theta, \boldsymbol{\Delta\theta}, \boldsymbol{\Delta\mathrm{SSe}}, \boldsymbol{\Delta\mathrm{SSe}})$, or

$$b(t) = \mathrm{eval}\Psi\left(\delta_\theta, \boldsymbol{\Delta\theta}, \boldsymbol{\Delta\mathrm{tSSe}}, \boldsymbol{\Delta\mathrm{SSe}}\right) \tag{26}$$

Then,

$$b(t) \subseteq \left[\underline{B(t)}, \overline{B(t)}\right] \tag{27}$$

as, $\left[\underline{B(t)}, \overline{B(t)}\right]$ is the interval evaluation $\boldsymbol{\Psi}$.

Now, $\forall t : t > 0$, for any $\boldsymbol{x} : \boldsymbol{x} \in \arg(\Psi)$, such that $\boldsymbol{x} \neq \boldsymbol{x}_n$ (i.e. when any parameter(s) or measurement(s) is not equal to its nominal value(s)), $\mathrm{eval}(R_n) \neq 0$ (nominal ARR value is ideally zero only when none of the uncertain candidates deviate from their respective nominal values).

Thus, as $b(t)$ is the numerical resultant of deviations on any (or all) of the uncertain candidates c.f. (26), following can be deduced:

$$\mathrm{eval}(R_n) + b(t) = 0 \tag{28}$$

$$\text{or, } b(t) = -r_n \tag{29}$$

From (29) and (27),

$$\left(-r_n(t)\right) \subseteq \left[\underline{B(t)}, \overline{B(t)}\right] \tag{30}$$

Hence, the interval range of URIF $\boldsymbol{\Psi}$ guarantees the containment of $\left(-r_n(t)\right)$, given that additive deviations of uncertain candidates remain within their pre-fixed interval bounds. □

Lemma 1. *Alternatively,* $\left(r_n(t)\right) \subseteq -\left[\underline{B(t)}, \overline{B(t)}\right]$.

Proof. This directly follows from Property B.3 (see Appendix B) such that,

$$\begin{aligned} &-r_n(t) \subseteq \left[\underline{B(t)}, \overline{B(t)}\right] \\ &\Rightarrow (-1)\left(-r_n(t)\right) \subseteq [-1,-1]\left[\underline{B(t)}, \overline{B(t)}\right] \\ &\Rightarrow r_n(t) \subseteq -\left[\underline{B(t)}, \overline{B(t)}\right] \quad \square \end{aligned} \tag{31}$$

Proposition 4. *If a fault is considered when one or more of the uncertain candidates sensitive to the given I-ARR, deviate out of their permissible interval limits, following are verified:*

- *Nominal conditions* $\left(-r_n(t)\right) \subset \left[\underline{B(t)}, \overline{B(t)}\right]$.
- *Fault detection if* $\left(-r_n(t)\right) \not\subset \left[\underline{B(t)}, \overline{B(t)}\right]$.

Proof. Proof directly follows from Proposition 3, where $-r_n(t) \subseteq \left[\underline{B(t)}, \overline{B(t)}\right]$ is verified if, for point valued variable vectors $\boldsymbol{\theta}, \delta_\theta, \boldsymbol{\theta}_n, \mathbf{SSe}(t)$, $\mathbf{SSf}(t), \boldsymbol{\Delta}\mathbf{SSe}, \boldsymbol{\Delta}\mathbf{SSe}$, following stands true: $\boldsymbol{\Delta\mathrm{SSe}} \in [-\boldsymbol{\Delta\mathrm{SSe}}_{\mathbf{l}}, \boldsymbol{\Delta\mathrm{SSe}}_{\mathbf{u}}]$, $\boldsymbol{\Delta\mathrm{SSf}} \in \left[-\boldsymbol{\Delta\mathrm{SSf}}_{\mathbf{l}}, \boldsymbol{\Delta\mathrm{SSf}}_{\mathbf{u}}\right]$, $\theta \in \left[\underline{\theta}, \bar{\theta}\right]$, $\delta_\theta \in \left[\underline{\delta_\theta}, \overline{\delta_\theta}\right]$

Lemma 3.2. *As it follows from Proposition 4 and Lemma 1:*

- *Under nominal conditions:* $r_n(t) \subseteq -\left[\underline{B(t)}, \overline{B(t)}\right]$ *is verified.*
- *A fault is detected if* $r_n(t) \not\subset -\left[\underline{B(t)}, \overline{B(t)}\right]$

Thus, in this section, a fault detection methodology is established where URIF $\left[\underline{B(t)}, \overline{B(t)}\right]$ of an I-ARR $\left[\underline{R(t)}, \overline{R(t)}\right]$, serves as threshold over nominal residual $R_n(t)$, robust to a given set of system parametric uncertainties and measurement uncertainties.

3.3. Resolution of interval dependency problem and implementation

One of the major problems encountered while evaluating the exact range of IEF is that of *interval dependency* (Moore et al., 2009) or *wrapping effect* in the set-theoretic context (Jaulin & Walter, 1993). This is mainly caused due to multiple occurrence or *multi-incidence* of an interval variable in expression of an IEF. The over-estimation of IEF range highly depends on the syntactic expression of the considered IEF (Hansen & Walster, 2003; Moore et al., 2009), that can be manipulated in an appropriate manner to incur minimal occurrences of interval variables in IEF. This can be achieved by using *nested form* which gives better range (and never worse) than *sum of powers* form, subdivision or *splitting* of domain arguments and union of IEF evaluations; *refinements* of IEF(s) and reduction of excess range width using *centred form*, *mean-value form*, *slope form*, *monotonicity-test form*; modal intervals involve the notion of *dual* intervals based upon monotonicity test etc.

In I-ARR context, the interval dependency problem can be tackled easily. It is assumed that only independent I-ARRs are derived. Redundant I-ARRs which can be obtained using combination of one or more independent I-ARRs are not considered in this work. The I-ARR at a detectable junction is generated by covering causal paths (Bouamama et al., 2003).

As such, multiple incidence of parametric uncertainty interval(s) (like $\left[\underline{\delta_R}, \overline{\delta_R}\right]$, c.f. (9)) would translate to the fact that either the same causal path has been covered more than once, or the same parameter occurs at multiple junctions. While the former implies presence of causal loop(s) leading to no subsequent I-ARR generation, the latter has little physical/practical relevance in the present context where distributed (not lumped) system models are not considered.

In this paper, the multi-incidence problem is alleviated by suitable manipulation of the syntactic expression of URIF such that there is minimal occurrence of an interval variable. In presence of multi-incident intervals, the N-IEF is algebraically manipulated and cast in nested form. Once this has been achieved, the URIF is expressed as finite sequence (commonly called a *computational graph or code list*) of interval arithmetic operations (see Appendix C). This is done to preserve the property of inclusion-isotonicity and validation of Proposition 2 (see Section 3.2). Moreover, it is assumed that arbitrarily sharp bounds can be computed for each of the unary functions (elementary type: $\exp(\cdot), ln(\cdot), \sqrt{\cdot}$) occurring in the *code lists.*

4. Case study on steam generator system

The FD method developed above is validated on an uncertain model of a steam generator system installed in CRIStAL laboratory. This system has well described along with associated BG model in Bouamama et al. (2000), Medjaher et al. (2006) and Ould Bouamama et al. (2006). The steam generator system as shown in Fig. 12 comprises of a feed water supply system, a tank, a pump, a pipe and a boiler of 55 kW and total volume of 0.170 m^3. The considered faults are: water leak in tank, valve blockage at pump outlet flow, water leak in boiler and fault on thermal resistor system.

4.1. Uncertain BG model

A detailed BG-LFT modelling of the system with parametric uncertainties, along with BG-LFT enabled robust diagnosis is described in Djeziri, Merzouki, et al. (2009) and Djeziri, Ould Bouamama, et al. (2009). The uncertain model developed in this work closely follows BG-LFT model developed in Djeziri, Merzouki, et al. (2009) and Djeziri, Ould Bouamama, et al. (2009). The deterministic (nominal) diagnostic BG in *preferred derivative causality* is given in Fig. 13. The uncertain BG which is constructed with interval-valued uncertain system parameters and measurements, is shown in Fig. 14

Although the basic structure of uncertain BG model remains similar to the BG-LFT one in Djeziri, Merzouki, et al. (2009) and Djeziri, Ould Bouamama, et al. (2009), there are some significant differences in terms of modelling and uncertainty quantification. The main differences are: interval models for parametric uncertainties and measurement uncertainties including the novel tank pressure sensor and tank-boiler

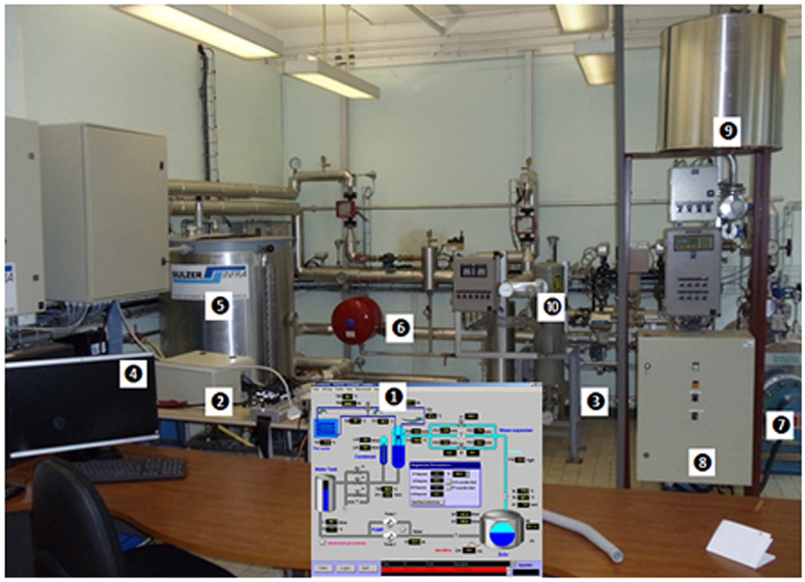

Fig. 12. Steam generator setup and supervision interface 1: Supervision interface 2: DSPACE data acquisition 3: Main power switch 4: Screen for monitoring 5: Water tank 6: Pump circuit 7: Boiler 8: Safety switch 9: Vapour output 10: Condenser and heat exchanger.

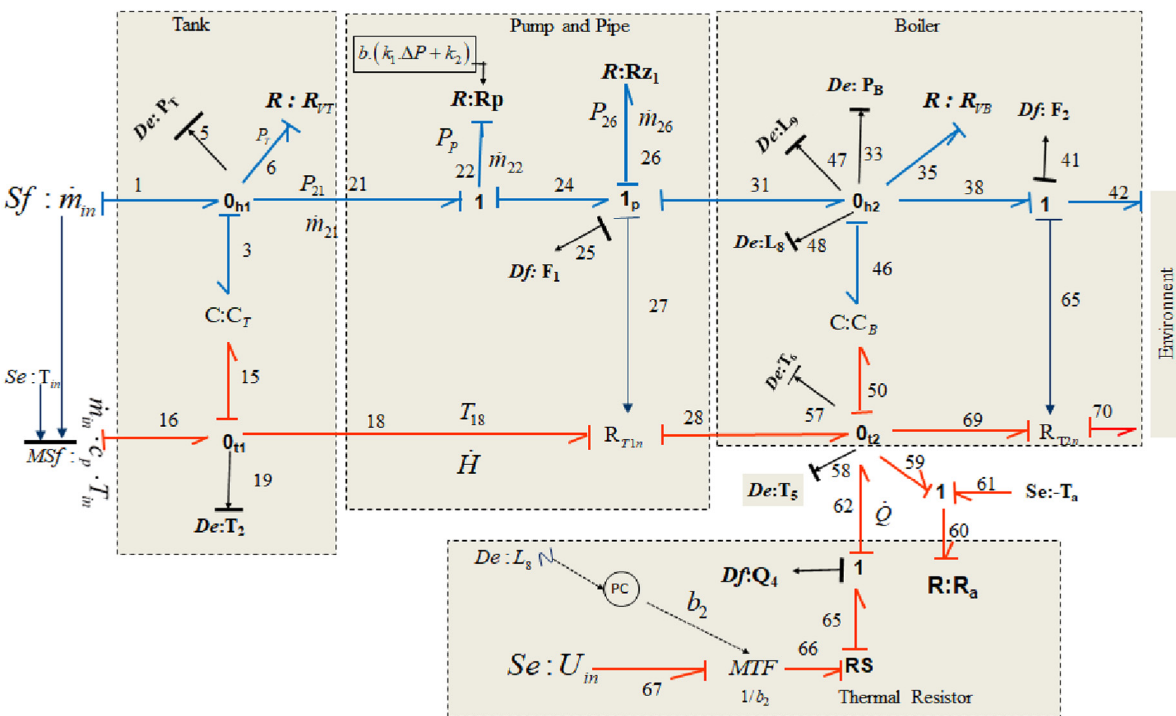

Fig. 13. Deterministic bond graph model of steam generator.

hydraulic valves, I-ARR generation and further IA based analysis. As the basic system dynamics remain similar to the one considered in Djeziri, Merzouki, et al. (2009) and Djeziri, Ould Bouamama, et al. (2009), description of the complete modelling procedure is omitted in this paper. Details about novel components are provided.

4.1.1. Tank

$De{:}P_T$ and $De{:}T_2$ represent the pressure sensor and temperature sensor present in the tank. Valve V_T present at the bottom of the tank is controlled manually to introduce water leakage in the tank. It represents a parametric fault. The mass flow rate, $\dot{m}_{vT}$, through the valve is given by the non-linear Bernoulli relation,

$$\begin{aligned} \dot{m}_{vT} &= Cd_T(x).sign(\Delta P).\sqrt{|\Delta P|} \\ \Delta P &= P_T - P_{atm} \end{aligned} \tag{32}$$

where ΔP is the pressure difference across the valve. x is the valve stem position between 0 and 1, where 0 means fully closed state and 1 implies fully open state. The installed characteristics are experimentally determined for four positions of the valve as shown in Table 1. Value of the Coefficient of discharge Cd_T is obtained for each of the valve positions.

Uncertainty on measurement of pressure sensor P_T is considered as,

$$\left[\underline{P_{T,m}}, \overline{P_{T,m}}\right] = P_{T,r} + \left[-\Delta P_{T,l}, \Delta P_{T,u}\right] \tag{33}$$

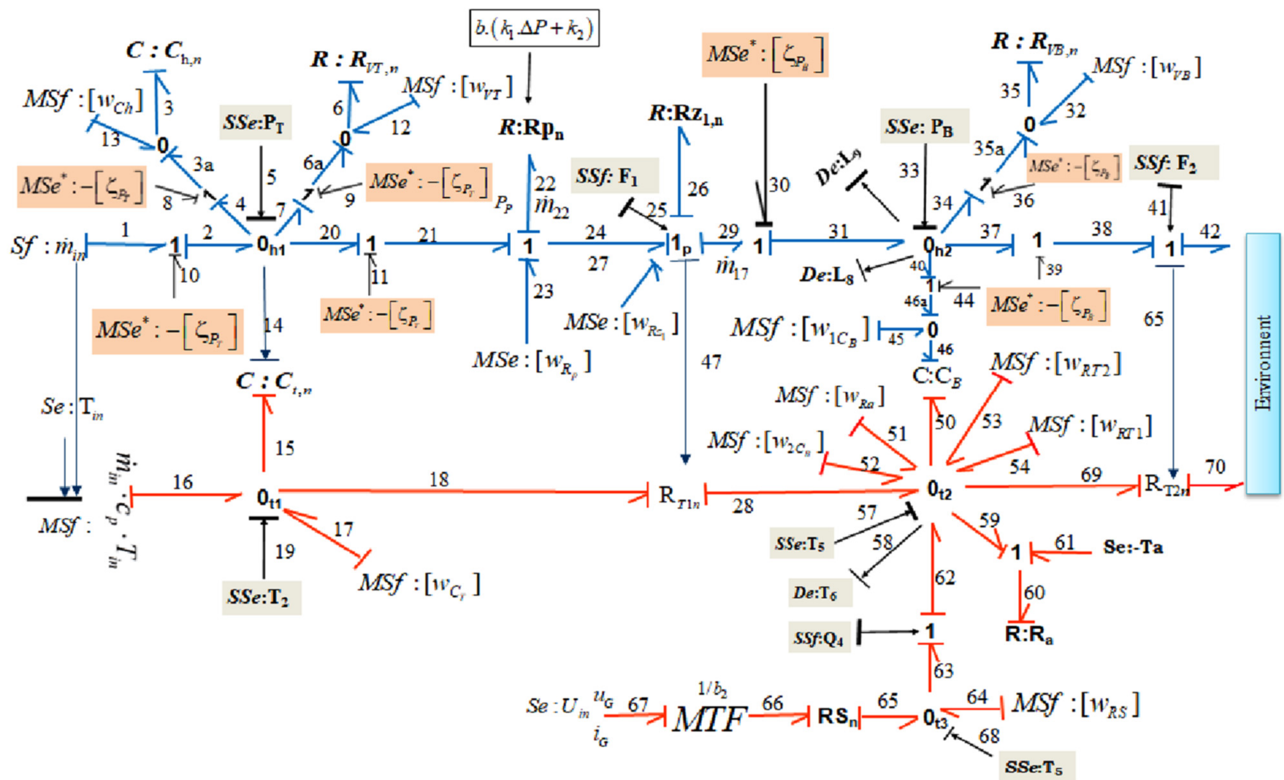

Fig. 14. Uncertain bond graph model of steam generator.

Table 1
Stem position of valve present in tank and discharge coefficient.

Valve stem position	$V_{T,1}$	$V_{T,2}$	$V_{T,3}$	$V_{T,4}$
Discharge coefficient	$Cd_{T,1}$ 6.32×10^{-3}	$Cd_{T,2}$ 6.678×10^{-3}	$Cd_{T,3}$ 6.987×10^{-3}	$Cd_{T,4}$ 7.14×10^{-3}

where $P_{T,m}$ is the measured signal (observed), $P_{T,r}$ is the true value of pressure (unobserved) and $\Delta P_{T,l}$ and $\Delta P_{T,u}$ are obtained from the *measurement error interval* provided by the manufacturer (± 1.5% of measured value). Measurement error is modelled in interval form : $[-\Delta P_{T,l}, \Delta P_{T,u}] \equiv [\zeta_{P_T}]$, represented as a modulated effort source $MSe^* : -[\zeta_{P_T}]$.

4.1.2. Pump and pipe system

The modelling of this sub-system can be referred in Djeziri, Merzouki, et al. (2009) and Djeziri, Ould Bouamama, et al. (2009).

4.1.3. Boiler

Boiler is instrumented with two redundant sensors of temperature $De\!:\!T_5$ and $De\!:\!T_6$, two redundant water level sensors $De\!:\!L_8$ and $De\!:\!L_9$, an uncertain pressure sensor $De\!:\!P_B$, a volumetric flow sensor at the output of the boiler $Df\!:\!F_2$, and a power sensor $Df\!:\!Q$.

Valve V_B present at the bottom of the tank is manually controlled and introduces water leakage (parametric fault) in the tank. The valve is modelled by non-linear resistor element $R\!:\!R_{VB}$ as,

$$f_{35} = \dot{m}_{vB} = Cd_B(x).sign(\Delta P).\sqrt{|\Delta P|} \tag{34}$$

$$\Delta P = e_{35} \tag{35}$$

where Cd_B is the coefficient of discharge proportional to the flow rate. The installed valve characteristics are determined experimentally for four valve positions as shown in Table 2.

During normal functioning of the system, stem positions are: $V_{B,1}$ and $V_{B,2}$. Thus, nominal value of discharge flow coefficient is $Cd_{B,1}$. The uncertainty in valve outflow is brought by inexact position of the valve stem (between $V_{B,1}$ and $V_{B,2}$). The latter is taken into account by limiting the variation of the discharge coefficient Cd_B, as $Cd_B \in [Cd_{B,1}, Cd_{B,2}]$ or $Cd_B = Cd_{B,1} + [0, \Delta Cd_B]$, where $\Delta Cd_B = Cd_{B2} - Cd_{B1}$. Thus, while $Cd_B \in [Cd_{B,1}, Cd_{B,2}]$, system is nominal with "no fault" in leakage. The corresponding uncertain flow $MSf\!:\![w_{VB}]$ (see f_{32} in Fig. 14) is determined as,

$$MSf : [w_{VB}] = -[0, \Delta Cd_B]\, sign(e_{35}).\sqrt{|e_{35}|} \tag{36}$$

Measurement from pressure sensor $SSe\!:\!P_B$ suffers the sensor bias (offset) and hence, it is considered uncertain as shown:

$$\left[\underline{P_{B,m}}, \overline{P_{B,m}}\right] = P_{B,r} + [-\Delta P_{B,l}, \Delta P_{B,u}] \tag{37}$$

Here, $P_{B,m}$ is the measured reading and $P_{B,r}$ is the actual reading. $[-\Delta P_{B,l}, \Delta P_{B,u}]$ models the uncertainty in the pressure measurement readings provided in the manufacturer's data-sheet.

4.1.4. Thermal resistor

The modelling of this sub-system can be referred in Djeziri, Merzouki, et al. (2009) and Djeziri, Ould Bouamama, et al. (2009).

4.2. I-ARR generation

I-ARRs are generated from the detectable junctions of each subsystem in Fig. 14. The concepts of interval $mid-point$ and interval $width$ are used to decouple nominal part and associated URIF.

I-ARR 1: For detection of leakage fault in the tank, energetic assessment at junction $\mathbf{0_{h1}}$ gives,

$$[\underline{R}_1, \overline{R}_1] = f_2 + f_5 - \left[\underline{f_4}, \overline{f_4}\right] - \left[\underline{f_7}, \overline{f_7}\right] - f_{20}$$

Table 2
Stem position of valve present in boiler and discharge coefficient.

Valve stem position	$V_{B,1}$	$V_{B,2}$	$V_{B,3}$	$V_{B,4}$
Discharge coefficient	$Cd_{B,1}$ 5.4678×10^{-3}	$Cd_{B,2}$ 5.78×10^{-3}	$Cd_{B,3}$ 6.278×10^{-3}	$Cd_{B,4}$ 6.478×10^{-3}

where

$$\begin{aligned}
&f_2=0, f_{20}=f_{24}=F_1, f_5=0,\\
&\left[\underline{f_7},\overline{f_7}\right]=Cd_{T,n}.sign(P_T).\left[\underline{\sqrt{|P_T-\Delta_{P_{T,u}}|}},\overline{\sqrt{|P_T+\Delta_{P_{T,l}}|}}\right]\\
&\quad+\left[0,Cd_{T,2}\right]sign(P_T).\left[\underline{\sqrt{|P_T-\Delta_{P_{T,u}}|}},\overline{\sqrt{|P_T+\Delta_{P_{T,l}}|}}\right]\\
&\left[\underline{f_4},\overline{f_4}\right]=\frac{A_{T,n}}{\rho_T g}.\frac{dP_T}{dt}+\left[\underline{\delta_{A_T}},\overline{\delta_{A_T}}\right].\frac{A_{T,n}}{\rho_T g}.\frac{dP_T}{dt}\\
&\quad+\left[\underline{A_T},\overline{A_T}\right].(1/\rho_T g).\frac{d[\zeta_{P_T}]}{dt}
\end{aligned}\tag{38}$$

The nominal residual $R_{1,n}$ and *URIF* $[\underline{B_1},\overline{B_1}]$ are determined as,

$$\begin{aligned}
R_{1,n}=&-\text{mid}\left(Cd_{T,n}.sign(P_T).\left[\underline{\sqrt{|P_T-\Delta_{P_{T,u}}|}},\overline{\sqrt{|P_T+\Delta_{P_{T,l}}|}}\right]\right)\\
&-\frac{A_{T,n}}{\rho_T g}.\frac{dP_T}{dt}-F_1
\end{aligned}\tag{39}$$

$$\begin{aligned}
\left[\underline{B_1},\overline{B_1}\right]=&-\left[0,Cd_{T,2}\right]sign(P_T).\left[\underline{\sqrt{|P_T-\Delta_{P_{T,u}}|}},\overline{\sqrt{|P_T+\Delta_{P_{T,l}}|}}\right]\\
&+-\left[\underline{\delta_{A_T}},\overline{\delta_{A_T}}\right].\frac{A_{T,n}}{\rho_T g}.\frac{dP_T}{dt}\\
&-\left[\underline{A_T},\overline{A_T}\right].(1/\rho_T g).\frac{d\left(\left[-\Delta P_{T,l},\Delta P_{T,u}\right]\right)}{dt}\\
&-\frac{1}{2}sign(P_T)Cd_{T,n}\left(\text{width}\left[\underline{\sqrt{|P_T-\Delta_{P_{T,u}}|}},\overline{\sqrt{|P_T+\Delta_{P_{T,l}}|}}\right]\right)\\
&\times[-1,1]
\end{aligned}\tag{40}$$

See Appendix C for the associated code list.

I-ARR 2: The second I-ARR is generated from the junction $\mathbf{1_p}$ connected to SSf: F_1. It is sensitive to fault due to valve blockage (or pipe plugging) at the pump output. Energetic assessment at $\mathbf{1_p}$ junction gives

$$\left[\underline{R_2},\overline{R_2}\right]=\left[\underline{e_{24}},\overline{e_{24}}\right]+\left[\underline{e_{25}},\overline{e_{25}}\right]-e_{26}-\left[\underline{e_{29}},\overline{e_{29}}\right]+\left[\underline{e_{27}},\overline{e_{27}}\right]$$

with $e_{26}=R_{z1}^2.F_1^2$, $\left[\underline{e_{29}},\overline{e_{29}}\right]=P_B-[\zeta_{P_B}]$, $\left[\underline{e_{27}},\overline{e_{27}}\right]=[w_{Rz1}]$,

$$\left[\underline{e_{24}},\overline{e_{24}}\right]=\left[\underline{e_{21}},\overline{e_{21}}\right]-\left[\underline{e_{22}},\overline{e_{22}}\right]+\left[\underline{e_{23}},\overline{e_{23}}\right]=(P_T-[\zeta_{P_T}])-\left((1/k_{1,n}).((\dot m_{22}/b)-k_{2,n})\right)+[w_{Rp}]$$

The *nominal residual* $R_{2,n}$ and *URIF* $[\underline{B_2},\overline{B_2}]$ are determined as,

$$R_{2,n}=P_T-(1/k_{1,n}).((\dot m_{22}/b)-k_{2,n})-R_{z1}^2.F_1^2-P_B\tag{41}$$

$$\begin{aligned}
[\underline{B_2},\overline{B_2}]=&\,MSe:[w_{Rz1}]+MSe:[w_{Rp}]-\left[-\Delta_{P_{T,l}},-\Delta_{P_{T,u}}\right]\\
&+\left[-\Delta_{P_{B,l}},-\Delta_{P_{B,u}}\right]\\
=&-2.\left[\underline{\delta_{R_{z1}}},\overline{\delta_{R_{z1}}}\right].R_{z1,n}.F_1^2-\frac{1}{k_{1,n}}.\left[\underline{\delta_{1/k_1}},\overline{\delta_{1/k_1}}\right]\left(\frac{\dot m_{22}}{b_1}-k_{2,n}\right)\\
&+\frac{k_{2,n}}{k_{1,n}}.\left[\underline{\delta_{k_2}},\overline{\delta_{k_2}}\right]\left(1+\left[\underline{\delta_{1/k_1}},\overline{\delta_{1/k_1}}\right]\right)\\
&-\left[-\Delta_{P_{T,l}},-\Delta_{P_{T,u}}\right]+\left[-\Delta_{P_{B,l}},-\Delta_{P_{B,u}}\right]
\end{aligned}\tag{42}$$

There will be *interval dependency* problem in range evaluation of (42) due to multi-incident interval $\left[\underline{\delta_{1/k_1}},\overline{\delta_{1/k_1}}\right]$. Thus, syntactic expression of IEF (42) is modified such that $\left[\underline{\delta_{1/k_1}},\overline{\delta_{1/k_1}}\right]$ occurs only once (minimum occurrence), as:

$$\begin{aligned}
[\underline{B_2},\overline{B_2}]=&-2.\left[\underline{\delta_{R_{z1}}},\overline{\delta_{R_{z1}}}\right].R_{z1,n}.F_1^2-.\left[\underline{\delta_{1/k_1}},\overline{\delta_{1/k_1}}\right]\\
&\times\left(\frac{1}{k_{1,n}}.\left(\frac{\dot m_{22}}{b_1}-k_{2,n}\right)-\frac{k_{2,n}}{k_{1,n}}.\left[\underline{\delta_{k_2}},\overline{\delta_{k_2}}\right]\right)\\
&+\frac{k_{2,n}}{k_{1,n}}.\left[\underline{\delta_{k_2}},\overline{\delta_{k_2}}\right]-\left[-\Delta_{P_{T,l}},-\Delta_{P_{T,u}}\right]+\left[-\Delta_{P_{B,l}},-\Delta_{P_{B,u}}\right]
\end{aligned}\tag{43}$$

See Appendix C for the associated code list.

I-ARR 3: Third I-ARR is generated from the junction $\mathbf{0_{h2}}$ connected to the dualized detector SSe:P_B sensitive to the leakage fault in the boiler.

$$\left[\underline{R_3},\overline{R_3}\right]=f_{31}-f_{37}-\left[\underline{f_{40}},\overline{f_{40}}\right]-\left[\underline{f_{34}},\overline{f_{34}}\right]$$

with

$$\left[\underline{f_{31}},\overline{f_{31}}\right]=\dot m_{31}=F_1,\left[\underline{f_{37}},\overline{f_{37}}\right]=\left[\underline{f_{38}},\overline{f_{38}}\right]=F_2,$$

$$\begin{aligned}
\left[\underline{f_{40}},\overline{f_{40}}\right]=&\,d\left(\rho_l(P_B).L_8+\rho_v(P_B).(V_B-L_8)\right)/dt+\left[\underline{\delta_{1,C_B}},\overline{\delta_{1,C_B}}\right]\\
&.\frac{d\left(\rho_{l,n}(P_B).V_{l,n}+\rho_{v,n}(P_B).V_{v,n}\right)}{dt}
\end{aligned}$$

$$\begin{aligned}
\left[\underline{f_{34}},\overline{f_{34}}\right]=&\,Cd_{B,n}.sign(P_B).\left[\underline{\sqrt{|P_B-\Delta_{P_{B,u}}|}},\overline{\sqrt{|P_B+\Delta_{P_{B,l}}|}}\right]\\
&+\left[0,Cd_{B,2}\right]sign(P_B).\left[\underline{\sqrt{|P_B-\Delta_{P_{B,u}}|}},\overline{\sqrt{|P_B+\Delta_{P_{B,l}}|}}\right]
\end{aligned}$$

The *nominal residual* $R_{3,n}$ and *URIF* $[\underline{B_3},\overline{B_3}]$ are determined as,

$$\begin{aligned}
R_{3,n}=&-d\left(\rho_l(P_B).L_8+\rho_v(P_B).(V_B-L_8)\right)/dt+F_1-F_2\\
&-\text{mid}\left[Cd_{B,n}.sign(P_B).\left[\underline{\sqrt{|P_B-\Delta_{P_{B,u}}|}},\overline{\sqrt{|P_B+\Delta_{P_{B,l}}|}}\right]\right]
\end{aligned}\tag{44}$$

$$\begin{aligned}
\left[\underline{B_3},\overline{B_3}\right]=&-\left[0,Cd_{B,2}\right]sign(P_B).\left[\underline{\sqrt{|P_B-\Delta_{P_{B,u}}|}},\overline{\sqrt{|P_B+\Delta_{P_{B,l}}|}}\right]\\
&-\left[\underline{\delta_{1,C_B}},\overline{\delta_{1,C_B}}\right].\frac{d\left(\rho_{l,n}(P_B).V_{l,n}+\rho_{v,n}(P_B).V_{v,n}\right)}{dt}\\
&-\frac{1}{2}Cd_{B,n}sign(P_B)\left(\text{width}\left[\underline{\sqrt{|P_B-\Delta_{P_{B,u}}|}},\overline{\sqrt{|P_B+\Delta_{P_{B,l}}|}}\right]\right)\\
&\times[-1,1]
\end{aligned}\tag{45}$$

See Appendix C for the associated code list.

I-ARR 4: Fourth I-ARR is generated from the thermal $\mathbf{0_{t2}}$ junction connected to the dualized SSe: T_5 as

$$\begin{aligned}
\left[\underline{R_4},\overline{R_4}\right]=&\,f_{28}+\left[\underline{f_{62}},\overline{f_{62}}\right]-f_{59}-f_{69}-\left[\underline{f_{50}},\overline{f_{50}}\right]\\
&+\left[\underline{f_{51}},\overline{f_{51}}\right]+\left[\underline{f_{52}},\overline{f_{52}}\right]+\left[\underline{f_{53}},\overline{f_{53}}\right]+\left[\underline{f_{54}},\overline{f_{54}}\right]
\end{aligned}$$

with,

$$f_{28}=\dot H_{28}=F_1.c_{p,n}.T_2,\left[\underline{f_{62}},\overline{f_{62}}\right]=\dot Q_4=(1/RS_n)U_{in}^2+MSf:[w_{RS}],$$

$$f_{59}=(1/R_{an})(T_5-Ta)$$

$$\begin{aligned}
f_{69}=&\,\dot H_{70}=T_5.c_{v,n}.F_2,\left[\underline{f_{50}},\overline{f_{50}}\right]\\
=&\,\frac{d\left(\rho_{l,n}(P_B).V_{l,n}.h_{l,n}(P_B)\right)}{dt}+\frac{d(\rho_{v,n}(P_B).V_{v,n}.h_{v,n}(P_B))}{dt}
\end{aligned}$$

$$\begin{aligned}
&\left[\underline{f_{51}},\overline{f_{51}}\right]=MSf:[w_{R_a}],\left[\underline{f_{52}},\overline{f_{52}}\right]=MSf:[w_{2C_B}],\left[\underline{f_{53}},\overline{f_{53}}\right]\\
&\quad=MSf:[w_{RT2}],\left[\underline{f_{54}},\overline{f_{54}}\right]=MSf:[w_{RT1}]
\end{aligned}$$

Table 3
Nominal values and uncertainty values.

	Physical name	Nominal value	Interval uncertainty	Uncertainty value		Physical name	Nominal value	Interval uncertainty	Uncertainty value
A_T	Tank Section	0.436 m^2	$[\underline{\delta_{A_T}}, \overline{\delta_{A_T}}]$	$[-0.004, 0.009]$	e_B	Thickness of the Boiler Metal	0.008 m	$[\underline{\delta_{e_B}}, \overline{\delta_{e_B}}]$	$[-0.085, 0.085]$
Cd_T	Discharge coefficient in Tank Valve	0.00632	$[0, \Delta Cd_T]$	$[0, 0.358 \times 10^{-3}]$	A_B	Boiler Section	1.887 m^2	$[\underline{\delta_{1/A_B}}, \overline{\delta_{1/A_B}}]$	$[-0.0067, 0.0067]$
$P_{T,m}$	Pressure in Tank	Measured	$[\underline{P_{T,m}}, \overline{P_{T,m}}]$	Measured	R_a	Heat transfer Parameter	2858 W/K	$[\underline{\delta_{1/R_a}}, \overline{\delta_{1/R_a}}]$	$[-0.0027, 0.0027]$
ΔP_T	Pressure Sensor Bias in Tank	Measured	$[\underline{\Delta P_T}, \overline{\Delta P_T}]$	$[-4.3, 4.9]$ Pa	V_B	Boiler Volume	0.175 m^3	0	0
c_p	Fluid specific Heat at constant Pressure	Variable	$[\underline{\delta_{c_p}}, \overline{\delta_{c_p}}]$	$[-0.015, 0.015]$	ρ_v	Steam Density	Variable	$[\underline{\delta_{\rho_v}}, \overline{\delta_{\rho_v}}]$	$[-0.02, 0.02]$
k_1	Pump Characteristic	-8.33×10^{-7} ms	$[\underline{\delta_{k_1}}, \overline{\delta_{k_1}}]$	$[-0.05, 0.05]$	h_v	Specific enthalpy of steam	Variable	$[\underline{\delta_{h_v}}, \overline{\delta_{h_v}}]$	$[-0.023, 0.023]$
k_2	Pump Characteristic	0.97 kg/s	$[\underline{\delta_{k_2}}, \overline{\delta_{k_2}}]$	$[-0.05, 0.05]$	h_l	Fluid specific enthalpy	Variable	$[\underline{\delta_{h_l}}, \overline{\delta_{h_l}}]$	$[-0.023, 0.023]$
R_{z1}	Pipe Hydraulic Resistance	2550 Pa s/kg	$[\underline{\delta_{R_{z1}}}, \overline{\delta_{R_{z1}}}]$	$[-0.01, 0.01]$	Cd_B	Discharge coefficient in Boiler Valve	0.00546	$[0, \Delta Cd_B]$	$[0, 0.284 \times 10^{-3}]$
λ	Thermal Conductivity of the boiler Wall	0.174 W/m K	$[\underline{\delta_{\lambda}}, \overline{\delta_{\lambda}}]$	0	$P_{T,m}$	Pressure in Boiler	Measured	$[\underline{P_{T,m}}, \overline{P_{T,m}}]$	[−1.2%, 1.2%]
RS	Thermal Electrical Resistance	2.406 Ω	$[\underline{\Delta RS}, \overline{\Delta RS}]$	$[0, 0.5]$	ΔP_T	Pressure Sensor Bias in Tank	Measured	$[\underline{\Delta P_T}, \overline{\Delta P_T}]$	$[-1.9, 1.9]$ Pa

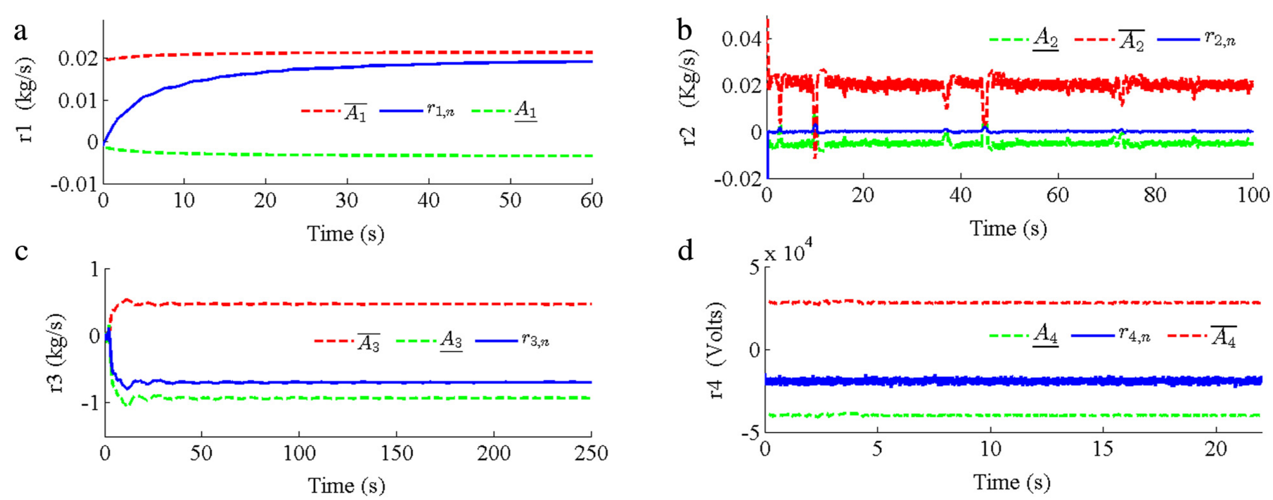

Fig. 15. Nominal conditions (a) Nominal residual $r_{1,n}$ and thresholds as range of $[\underline{A_1}, \overline{A_1}] = -[\underline{B_1}, \overline{B_1}]$; (b) Nominal residual $r_{2,n}$ and thresholds as range of $[\underline{A_2}, \overline{A_2}] = -[\underline{B_2}, \overline{B_2}]$, (c) Nominal residual $r_{3,n}$ and thresholds as range of $[\underline{A_3}, \overline{A_3}] = -[\underline{B_3}, \overline{B_3}]$, (d) Nominal residual $r_{4,n}$ and thresholds as range of $[\underline{A_4}, \overline{A_4}] = -[\underline{B_4}, \overline{B_4}]$.

The *nominal residual* $R_{4,n}$ and URIF $[\underline{B_4}, \overline{B_4}]$ are determined as,

$$R_{4,n} = F_1.c_{p,n}.T_2 + (1/RS_n)U_{in}^2 - (1/R_{an})(T_5 - Ta) \\ -T_6.c_{v,n}.F_2 - \frac{d\left(\rho_{l,n}(P_B).V_{l,n}.h_{l,n}(P_B)\right)}{dt} - \frac{d(\rho_{v,n}(P_B).V_{v,n}.h_{v,n}(P_B))}{dt} \tag{46}$$

$$\begin{aligned}[\underline{B_4}, \overline{B_4}] &= [w_{RT1}] + [w_{RS}] + [w_{2C_B}] + [w_{RT2}] + [w_{R_a}] \\ &= \left[\underline{\delta_{c_p}}, \overline{\delta_{c_p}}\right] c_{p,n}.T_2.F_1 + b_2.\left[\underline{\delta_{1/RS}}, \overline{\delta_{1/RS}}\right] \frac{U_{in}^2}{RS_n} \\ &\quad - \left[\underline{\delta_{2,C_B}}, \overline{\delta_{2,C_B}}\right] \frac{d(\rho_{l,n}(P_B).V_{l,n}.h_{l,n}(P_B) + \rho_{v,n}(P_B).V_{v,n}.h_{v,n}(P_B))}{dt} \\ &\quad - \left[\underline{\delta_{c_v}}, \overline{\delta_{c_v}}\right].c_{v_n}.T_6.F - \left[\underline{\delta_{1/R_a}}, \overline{\delta_{1/R_a}}\right](1/R_{an}).(T_5 - T_a)\end{aligned} \tag{47}$$

See Appendix C for the associated code list.

Remark. In this paper, the derivative of any interval $[-\Delta_l, \Delta_u]$ is evaluated as,

$$\frac{d\left([-\Delta_l, \Delta_u]\right)}{dt} = \frac{\left([-\Delta_l, \Delta_u]_{t_i} - [-\Delta_l, \Delta_u]_{t_{i-1}}\right)}{t_i - t_{i-1}} \tag{48}$$

where the uncertainty interval $[-\Delta_l, \Delta_u]$ is considered time-invariant. It is calculated as

$$[-\Delta_l, \Delta_u]_{t_i} - [-\Delta_l, \Delta_u]_{t_{i-1}} = [-\Delta_l - \Delta_u, \Delta_u + \Delta_l] \tag{49}$$

4.3. Experimental results

The nominal and uncertainty values are tabulated in Table 3. The interval computations are achieved using INTLAB (Rump, 1999) library, which is a toolbox for MATLAB supporting real and complex interval computations. The real time computation are done using dSPACE® real time interface implemented via SIMULINK.

Nominal Conditions. Fig. 15 shows the four residuals found in the previous section, under no fault conditions, with all the parameters remaining inside their pre-defined interval bounds. The latter translate to the following facts:

- Stem position of the valve V_T is between $V_{T,1}$ (discharge coefficient $Cd_{T,1}$) and $V_{T,2}$ (discharge coefficient $Cd_{T,2}$).
- Stem position of the valve V_B is between $V_{B,1}$ (discharge coefficient $Cd_{B,1}$) and the position $V_{B,2}$ (discharge coefficient $Cd_{B,2}$)
- None of the system parameters are modulated manually.

Fault in tank. Fig. 16(a) shows the variation in outflow from valve V_T. At $t = 6$ s, the valve stem position is manually changed from its nominal state (between $V_{T,1}$ and $V_{T,2}$) to $V_{T,3}$ (see Table 1). This leads to increase in the flow output as shown in Fig. 16(a). The latter translates to the fact that associated discharge coefficient Cd_T is outside of the allowed interval limits i.e. $Cd_T \notin [Cd_{T,1}, Cd_{T,2}]$.

Fault in pipe. As shown in Fig. 17(a), the resistance of the pipe is increased by modulating the stopper at the output of the pump. The volumetric flow is measured by $Df : F_1$ (kg/s). As shown in Fig. 17(b), the parametric deviation (fault) results in deviation of $r_{2,n}$ outside the associated URIF bounds.

Fault in boiler. Fig. 18(a) shows the variation in outflow of valve V_B. The valve stem position is manually changed between $t = 30$ s and $t = 110$ s; the nominal state (between $V_{B,1}$ and $V_{B,2}$) is modulated to $V_{B,3}$ (see Table 2). The fault is detected when the corresponding nominal residual $r_{3,n}$ deviates outside the bounds of associated URIF, as shown in Fig. 18(b).

Fault in the thermal resistor. In Fig. 19(a), value of the thermal resistor (electrical resistance) is modulated linearly between $t = 13$ s and $t = 22$. The corresponding upper limit of +0.5 ohm is passed at around $t = 16$ s. As shown in Fig. 19(b), $r_{3,n}$ deviates outside the upper threshold limit and thus, fault is detected. The residual is corrupted with sensor noise (visible as sharp peaks).

5. Comparison with BG-LFT enabled Robust FDI

Consider a parameter vector θ and two uncertain parameters $\theta_1, \theta_2 \in \boldsymbol{\theta}$. Without the loss of generality, it is assumed that energetic assessment is done at a 1-*junction* to obtain: (i) BG-LFT derived ARR: R_{BG-LFT} and, (ii) uncertain BG derived I-ARR: $[\underline{R}, \overline{R}]$. Moreover, it is assumed there are only two uncertain system parameters $\{\theta_1, \theta_2\} \in \boldsymbol{\theta}$ sensitive to R and $[\underline{R}, \overline{R}]$.

BG-LFT method. In BG-LFT context, an uncertain parameter θ_i, (i= 1, 2) can be modelled as:

$$\theta_i = \theta_{i,n} \pm \Delta\theta_i; \quad \Delta\theta_i \geq 0 \tag{50}$$

$$\text{or}, \theta_i = \theta_{i,\mathrm{n}}(1 \pm \delta_{\theta_i}); \; \delta_{\theta_i} = \frac{\Delta\theta_i}{\theta_{i,n}} \tag{51}$$

where $\Delta\theta_i$ is the additive uncertainty, quantified statistically and δ_{θ_i} is the corresponding multiplicative uncertainty. The lower and upper limits on the parametric deviation remain equal. The associated ARR: R_{BG-LFT} consists of nominal part r_{BG-LFT} and uncertain part b_{BG-LFT} as $R_{BG-LFT} = r_{BG-LFT} + b_{BG-LFT}$. The nominal part is sensitive to nominal parametric value and uncertain part b is sensitive to parametric uncertainties and uncertain efforts/flows, brought by the respective parametric uncertainties. Thus,

$$b = w_{\theta_1} + w_{\theta_2} \tag{52}$$

where uncertain efforts are : $w_{\theta_1} = \Delta_{\theta_1} e_{\theta_1}$ and $w_{\theta_2} = \Delta_{\theta_2}.e_{\theta_2}$; with e_{θ_i} being the effort brought by the additive uncertainty Δ_{θ_i} on θ_i at the 1 junction. Then, lower threshold a_{lower} and upper threshold a_{upper} are formed as:

$$a_{upper} = |w_{\theta_1}| + |w_{\theta_2}| = |\Delta\theta_1.e_{\theta_1}| + |\Delta\theta_2 e_{\theta_2}| = \Delta\theta_1|e_{\theta_1}| + \Delta\theta_2|e_{\theta_2}| \tag{53}$$

$$a_{lower} = -a_{upper} = -\Delta\theta_1|e_{\theta_1}| - \Delta\theta_2|e_{\theta_2}| \tag{54}$$

Clearly, thresholds are sensitive to absolute values of uncertain efforts. Therefore, the sign (mutual influence) of uncertain efforts/flows are not taken into account during the development of thresholds.

I-ARR context. Uncertain parameters as interval models only require the knowledge of interval bounds. As such, knowledge of statistical properties (probabilistic distribution) of uncertainty are not needed. Following the I-ARR generation method presented before, I-ARR: $[\underline{R}, \overline{R}]$ has URIF as,

$$[\underline{B}, \overline{B}] = [-\Delta\theta_{1,l}, \Delta\theta_{1,u}]\, e_{\theta_1} + [-\Delta\theta_{2,l}, \Delta\theta_{2,u}]\, e_{\theta_2} \tag{55}$$

Clearly, the signs of efforts e_{θ_i}, (i =1, 2) are taken into account for determination of threshold limits. Moreover, interval arithmetic is involved in the determination of the range of URIF (interval limits).

For comparative purposes, the uncertain parts produced by BG-LFT method and I-ARR methods are shown in Table 4. Intuitively, owing to interval computations, interval uncertain part leads to thresholds that are more robust to false alarms than BG-LFT ones.

Table 4
Uncertain parts produced in ARRs by BG-LFT method and I-ARR method.

BG-LFT method	I-ARR method
$b = \Delta_{\theta_1} e_{\theta_1} + \Delta_{\theta_2}.e_{\theta_2}$	$[\underline{B}, \overline{B}] = [-\Delta\theta_{1,l}, \Delta\theta_{1,u}]\, e_{\theta_1} + [-\Delta\theta_{2,l}, \Delta\theta_{2,u}]\, e_{\theta_2}$

The upper and lower thresholds generated from the interval bounds of the range of URIFs, for different sign configurations of uncertain efforts, are shown in Table 5.

Herein, it is observed that when the bounds of the interval uncertainty are kept symmetric (lower limit equals upper limit), the upper and lower thresholds obtained from URIF range values, are equal to the one produced by BG-LFT method.

Thus, given that if rounding errors are ignored, BG-LFT based uncertainty-quantification and threshold-generation become special cases within I-ARR framework, where uncertainty interval limits remain symmetric with respect to the nominal value (centre of the interval) of an uncertain component. A similar analysis can be exercised at 0-*junction* with more than two uncertain parameters.

5.1. BG-LFT enabled threshold generation for steam generator system

In the context of steam generator, BG-LFT enabled thresholds are generated from the four sub-systems considered in Section 4.1. To that end, each of the uncertain parameters is considered with symmetric uncertainty limits. Moreover, the physical processes that deviate unidirectionally are considered in a way such that uncertainty limits are symmetric with respect to their respective nominal values.

Parametric values that have been modified for BG-LFT threshold generation are listed in Table 6. Table 7 lists BG-LFT thresholds associated with each of the residuals derived from the four sub-systems.

The four residuals are shown with their URIFs and BG-LFT enabled thresholds in Fig. 20 and Fig. 21.

Following observations can be made from Fig. 20 and Fig. 21:

- As observed in Fig. 20(b), Fig. 20(d), Fig. 21(b), and Fig. 21(d), the BG-LFT generated thresholds are symmetric in nature. Moreover, the width of the thresholds is greater in magnitude than their corresponding interval-valued ones.
- In the presence of mutually-compensating uncertain effort(s)/flow(s), I-ARRs are successful in generating optimal thresholds. On the contrary, BG-LFT method produces over-estimated thresholds that

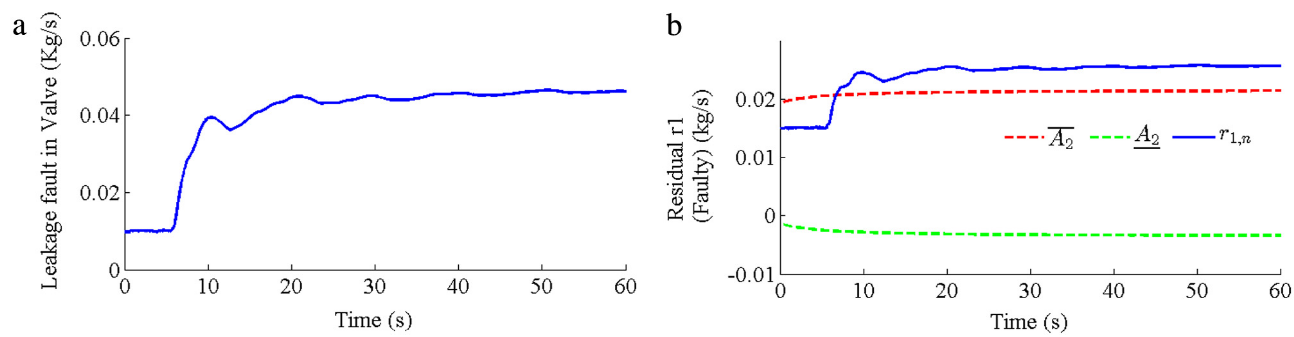

Fig. 16. Fault in water tank (a) Leakage of water (b) Fault detection with nominal residual $r_{1,n}$ and thresholds as range of $\left[\underline{A_1},\overline{A_1}\right] = -\left[\underline{B_1},\overline{B_1}\right]$.

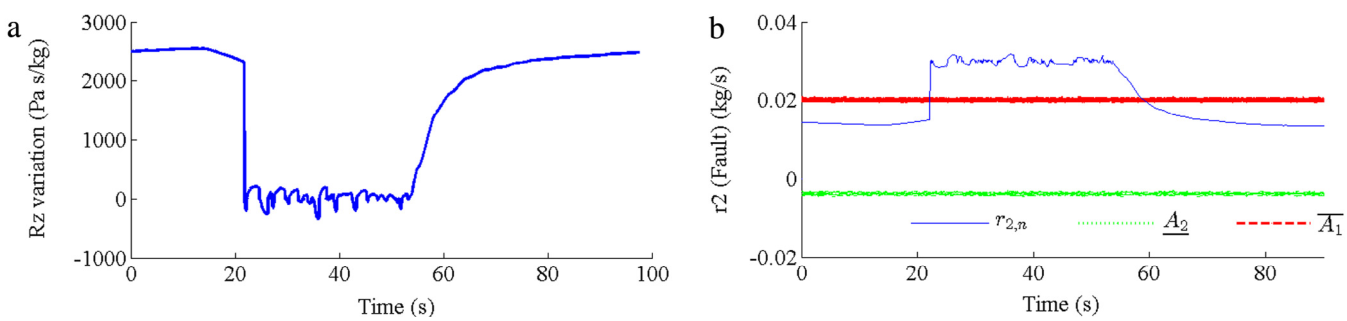

Fig. 17. Fault in pipe (a) Variation of resistance R_z (b) Fault detection with nominal residual $r_{2,n}$ and thresholds as range of $\left[\underline{A_2},\overline{A_2}\right] = -\left[\underline{B_2},\overline{B_2}\right]$.

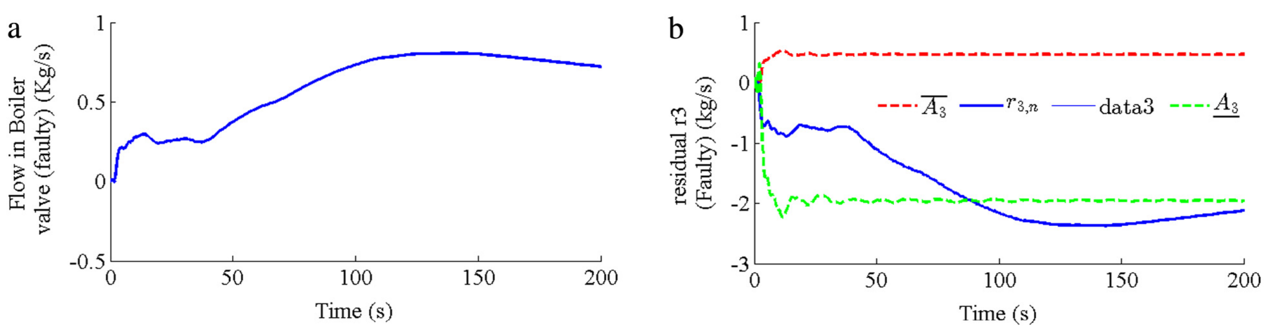

Fig. 18. Fault in boiler valve V_B (a) Water leakage (b) Fault detection with nominal residual $r_{3,n}$ and thresholds as range of $\left[\underline{A_3},\overline{A_3}\right] = -\left[\underline{B_3},\overline{B_3}\right]$.

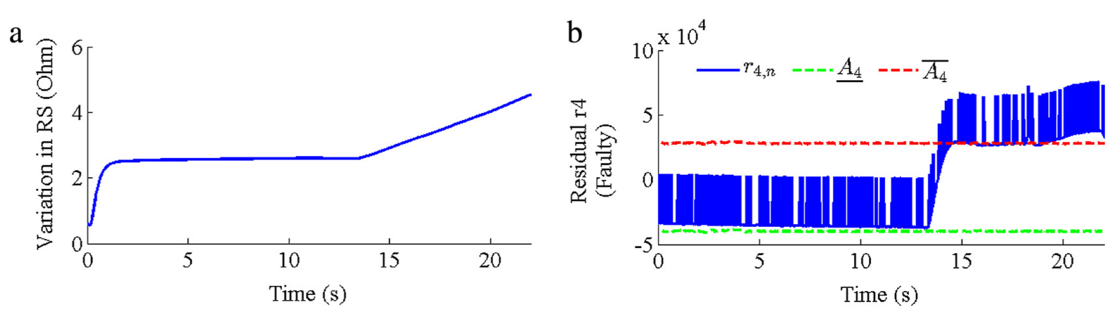

Fig. 19. Fault in electrical resistor (a) Increase in the resistance RS (b) Fault detection with nominal residual $r_{4,n}$ and thresholds as range of $\left[\underline{A_4},\overline{A_4}\right] = -\left[\underline{B_4},\overline{B_4}\right]$.

may lead to non-detection of fault. For example, $r_{4,n}$ is sensitive to uncertain candidates that are mutually compensating in nature (positively and negatively sensitive to nominal residual, see (47)). The I-ARR enabled URIFs lead to efficient threshold bounds as shown in Fig. 21(c). On the other hand, BG-LFT involves the naive summation of the absolute values of each uncertain flow/effort that results in over-estimated thresholds. It leads to non-detection of the fault as shown in Fig. 21(d).

- With respect to $r_{1,n}, r_{2,n}$ and $r_{3,n}$, I-ARR enabled URIFs and BG-LFT thresholds are successful in fault detection. This is due to the fact that parametric uncertainties involved in their corresponding URIFs are not mutually compensating in nature (see (40), (42) and (45)).

Table 5
URIF bounds and BG-LFT thresholds with symmetric and non-symmetric interval uncertainty.

Possible sign configuration of efforts	URIF Range interval limits	URIF Range interval limits with symmetric interval uncertainty $\Delta\theta_1 = \Delta\theta_{1,l} = \Delta\theta_{1,u}$ $\Delta\theta_2 = \Delta\theta_{2,1} = \Delta\theta_{2,u}$	BG-LFT thresholds (Symmetric uncertainty limits) $\pm\Delta\theta_1, \pm\Delta\theta_2$
$e_{\theta_1} \geq 0, e_{\theta_2} \geq 0$	$\underline{B} = -\Delta\theta_{1,l}.e_{\theta_1} - \Delta\theta_{2,l}e_{\theta_2}$ $\overline{B} = \Delta\theta_{1,u}.e_{\theta_1} + \Delta\theta_{2,u}e_{\theta_2}$	$\underline{B} = -\Delta\theta_1.e_{\theta_1} - \Delta\theta_2 e_{\theta_2}$ $\overline{B} = \Delta\theta_1.e_{\theta_1} + \Delta\theta_2 e_{\theta_2}$	$a_{lower} = -\Delta\theta_1 \lvert e_{\theta_1}\rvert - \Delta\theta_1 \lvert e_{\theta_2}\rvert$ $a_{upper} = \Delta\theta_1 \lvert e_{\theta_1}\rvert + \Delta\theta_1 \lvert e_{\theta_2}\rvert$
$e_{\theta_1} \geq 0, e_{\theta_2} \leq 0$	$\underline{B} = -\Delta\theta_{1,l}\lvert e_{\theta_1}\rvert - \Delta\theta_{2,u}\lvert e_{\theta_2}\rvert$ $\overline{B} = \Delta\theta_{1,u}\lvert e_{\theta_1}\rvert + \Delta\theta_{2,1}\lvert e_{\theta_2}\rvert$	$\underline{B} = -\Delta\theta_1\lvert e_{\theta_1}\rvert - \Delta\theta_2\lvert e_{\theta_2}\rvert$ $\overline{B} = \Delta\theta_1\lvert e_{\theta_1}\rvert + \Delta\theta_2\lvert e_{\theta_2}\rvert$	$a_{lower} = -\Delta\theta_1 \lvert e_{\theta_1}\rvert - \Delta\theta_1 \lvert e_{\theta_2}\rvert$ $a_{upper} = \Delta\theta_1 \lvert e_{\theta_1}\rvert + \Delta\theta_1 \lvert e_{\theta_2}\rvert$
$e_{\theta_1} \leq 0, e_{\theta_2} \geq 0$	$\underline{B} = -\Delta\theta_{1,u}.\lvert e_{\theta_1}\rvert - \Delta\theta_{2,l}\lvert e_{\theta_2}\rvert$ $\overline{B} = \Delta\theta_{1,1}.\lvert e_{\theta_1}\rvert + \Delta\theta_{2,u}\lvert e_{\theta_2}\rvert$	$\underline{B} = -\Delta\theta_1.\lvert e_{\theta_1}\rvert - \Delta\theta_2\lvert e_{\theta_2}\rvert$ $\overline{B} = \Delta\theta_1.\lvert e_{\theta_1}\rvert + \Delta\theta_2\lvert e_{\theta_2}\rvert$	$a_{lower} = -\Delta\theta_1 \lvert e_{\theta_1}\rvert - \Delta\theta_1 \lvert e_{\theta_2}\rvert$ $a_{upper} = \Delta\theta_1 \lvert e_{\theta_1}\rvert + \Delta\theta_1 \lvert e_{\theta_2}\rvert$
$e_{\theta_1} \leq 0, e_{\theta_2} \leq 0$	$\underline{B} = -\Delta\theta_{1,u}.\lvert e_{\theta_1}\rvert - \Delta\theta_{2,u}\lvert e_{\theta_2}\rvert$ $\overline{B} = \Delta\theta_{1,1}.\lvert e_{\theta_1}\rvert + \Delta\theta_{2,1}\lvert e_{\theta_2}\rvert$	$\underline{B} = -\Delta\theta_1.\lvert e_{\theta_1}\rvert - \Delta\theta_2\lvert e_{\theta_2}\rvert$ $\overline{B} = \Delta\theta_1.\lvert e_{\theta_1}\rvert + \Delta\theta_2\lvert e_{\theta_2}\rvert$	$a_{lower} = -\Delta\theta_1 \lvert e_{\theta_1}\rvert - \Delta\theta_1 \lvert e_{\theta_2}\rvert$ $a_{upper} = \Delta\theta_1 \lvert e_{\theta_1}\rvert + \Delta\theta_1 \lvert e_{\theta_2}\rvert$

Table 6
Uncertainty values for BG-LFT type threshold generation.

	Physical name	Nominal value	Interval uncertainty	BG-LFT uncertainty
A_T	Tank Section	0.436 m^2	$\left[\underline{\delta_{A_T}}, \overline{\delta_{A_T}}\right] = [-0.004, 0.009]$	$\pm\delta_{A_T} = 0.009$
Cd_T	Discharge coefficient in tank valve	0.623	$[0, \Delta Cd_T] = [0, 0.358 \times 10^{-3}]$	$\pm\Delta Cd_T = \pm 0.358 \times 10^{-3}$
RS	Thermal electrical resistance	2.406 Ω	$\left[\underline{\Delta RS}, \overline{\Delta RS}\right] = [0, 0.5]$	$\pm\Delta RS = \pm 0.5$
Cd_B	Discharge coefficient in boiler valve	0.61	$[0, \Delta Cd_B] = [0, 0.284 \times 10^{-3}]$	$\pm\Delta Cd_B = \pm 0.284 \times 10^{-3}$

Table 7
Threshold generation using BG-LFT method.

Residual	Uncertain part	BG-LFT thresholds
$r_{1,n}$	$a_1 = \lvert Cd_{T,2}sign(P_T - \Delta_{P_T}).\sqrt{\lvert P_T - \Delta_{P_T}\rvert}\rvert + \lvert\delta_{A_T}\cdot\frac{A_{T,n}}{\rho_T g}\cdot\frac{dP_T}{dt}\rvert + \lvert(A_{T,n} + \delta_{A_T} A_{T,n})(1/\rho_T g).2.\frac{\Delta_{P_T}}{\Delta t}\rvert$	$-a_1 \leq r_{1,n} \leq a_1$
$r_{2,n}$	$a_2 = \lvert w_{Rz1}\rvert + \lvert w_{Rp}\rvert + \max\lvert\Delta_{P_T}\rvert + \max\lvert\Delta_{P_B}\rvert$	$-a_2 \leq r_{2,n} \leq a_2$
$r_{3,n}$	$a_3 = \lvert Cd_{B,1}.sign(P_B - \Delta P_B).\sqrt{\lvert P_B - \Delta P_B\rvert}\rvert + \lvert\delta_{1,C_B}\cdot\frac{d\left(\rho_{l,n}(P_B).V_{l,n} + \rho_{v,n}(P_B).V_{v,n}\right)}{dt}\rvert$	$-a_3 \leq r_{3,n} \leq a_3$
$r_{4,n}$	$a_4 = \lvert w_{RT1}\rvert + \lvert w_{RS}\rvert + \lvert w_{RT2}\rvert + \lvert w_{R_a}\rvert + \lvert w_{2C_B}\rvert$	$-a_4 \leq r_{4,n} \leq a_4$

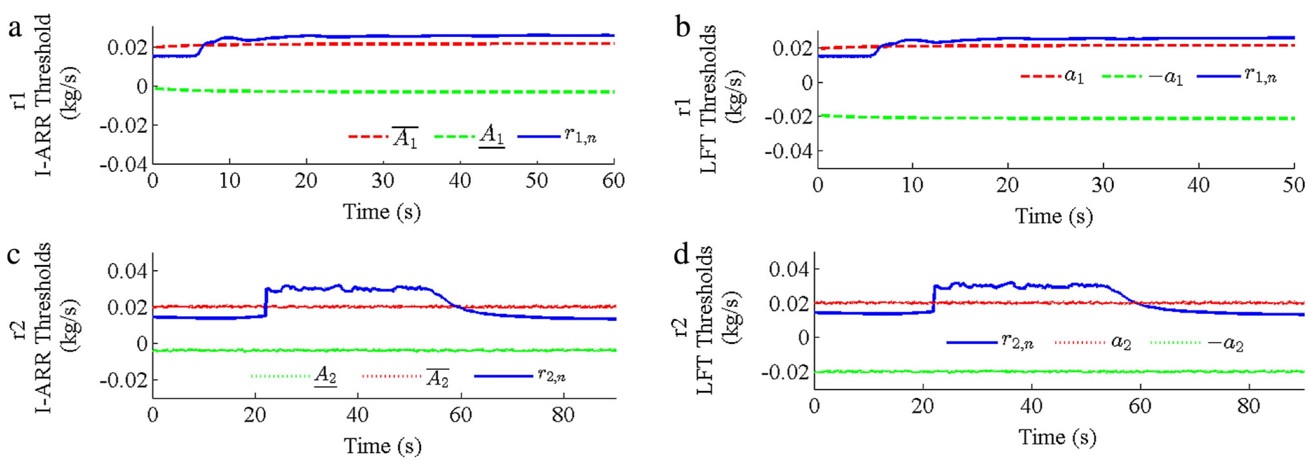

Fig. 20. (a) Fault detection with nominal residual $r_{1,n}$ and thresholds as range of $\left[\underline{A_1}, \overline{A_1}\right] = -\left[\underline{B_1}, \overline{B_1}\right]$ (b) Fault detection with nominal residual $r_{1,n}$ and $-a_1, a_1$ as BG-LFT Thresholds (c) Fault detection with nominal residual $r_{2,n}$ and thresholds as range of $\left[\underline{A_2}, \overline{A_2}\right] = -\left[\underline{B_2}, \overline{B_2}\right]$ (d) Fault detection with nominal residual $r_{2,n}$ and $-a_2, a_2$ as BG-LFT thresholds.

6. Conclusions

- This paper builds the framework of modelling the uncertain system parameters as well as uncertain sensor measurements in interval form on uncertain BG models. An attempt has been made to integrate the advantages of BG models and properties of IA.
- In particular, the structural and causal properties of BGs are exploited to generate I-ARRs. These I-ARRs can be decoupled into *nominal residuals* and URIFs using some specific properties of interval arithmetic. A sequence of steps, URIFs lead to development of efficient thresholds that must contain the *nominal residuals* under nominal system functioning.
- This work alleviates the limitations associated with the existing method of uncertain diagnosis based upon BG-LFT. Moreover, it has been shown that BG-LFT method based uncertainty quantification and threshold generation, are special cases within I-ARR framework, when the uncertainty interval limits are symmetric with respect to the nominal value of the considered uncertain candidate.
- The experimental study has demonstrated the viability of I-ARR based method. In the presence of mutually compensating uncertain system variables (effort/flows), I-ARRs are successful in producing optimal thresholds; on the contrary, BG-LFT enabled

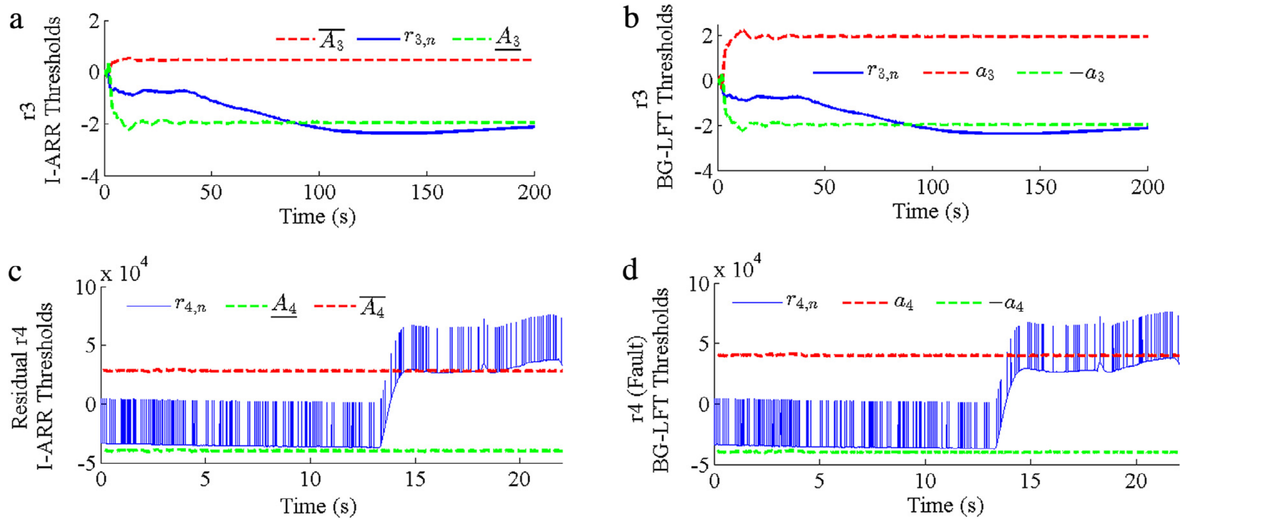

Fig. 21. (a) Fault detection with nominal residual $r_{3,n}$ and thresholds as range of $\left[\underline{A_3}, \overline{A_3}\right] = -\left[\underline{B_3}, \overline{B_3}\right]$ (b) Fault detection with nominal residual $r_{3,n}$ and $-a_3, a_3$ as BG-LFT thresholds (c) Fault detection with nominal residual $r_{4,n}$ and thresholds as range of $\left[\underline{A_4}, \overline{A_4}\right] = -\left[\underline{B_4}, \overline{B_4}\right]$ (d) Non detection of fault with nominal residual $r_{4,n}$ and $-a_4, a_4$ as BG-LFT thresholds.

thresholds are generally over-bounded leading to non-detection of fault.

- This work forms the initial step towards integrating interval analysis based capabilities in BG framework for fault detection and health monitoring of uncertain systems. In future, various other set membership based methods will be integrated using the framework presented here. In this work, issue of *interval dependency* is resolved by suitable manipulation of syntactic expression of interval functions. In future, other ways of dealing with interval dependency problem will be analysed such as modal intervals, set inversion techniques, centred forms etc. Additionally, various other technique to estimate the derivative of interval variable will be explored and integrated within this framework.

Acknowledgements

The first author is thankful to Prof. Genevieve Dauphin-Tanguy and Ecole Centrale de Lille, for funding the research work.

Appendix A. Basics of bond graph modelling

BG is a topological modelling language. The energy exchange link is called a *bond* with generic power variables named *effort* e and *flow* f, associated with every bond, such that $e \times f = Power$. The set of elements $\{I, C, R\}$ models the system parameters/component where I, C, and R are the *inertial* element, *capacitance* element and *dissipation* element respectively. The latter along with the elements $\{0, 1, TF, GY\}$ define the junction structure (global structure of the system) where TF and GY are the *transformer* element and *gyrator* element respectively. Junction **0** (or **1**) implies that all the connected bonds have same *effort* (or *flow*) and the sum of *flows* (or *efforts*) equals zero. The constitutive equations of I and C respectively, in integral causality are (linear case) : $f(t) = (1/I)\int e(t)dt$ and $e(t) = (1/C)\int f(t)dt$. *Derivative causality* dictates the constitutive equation of I and C respectively, to be as (linear case): $e(t) = I\, d(f(t))/dt$ and $f(t) = C\, d(e(t))/dt$.

Appendix B. Interval analysis

Definitions and properties listed below can be found in Moore et al. (2009).

Definition B.1. For the interval X, *midpoint* of X is given by

$$\text{mid}(X) = \frac{1}{2}\left(\overline{X} + \underline{X}\right)$$

Definition B.2. For any interval X, the *width* of the interval is defined and denoted by

$$\text{width}(X) = \overline{X} - \underline{X}$$

Property B.1. Any interval X can be expressed as,

$$\begin{aligned} X &= \text{mid}(X) + \left[-\frac{1}{2}\text{width}(X), \frac{1}{2}\text{width}(X)\right] \\ &= \text{mid}(X) + \frac{1}{2}\text{width}(X)[-1, 1] \end{aligned}$$

Property B.2 (*Interval Arithmetic Operations*). For two intervals X and Y such that, $\{x|\underline{X} \le x \le \overline{X}\}$ and $\{y|\underline{Y} \le y \le \overline{Y}\}$

- $X + Y = \left[\underline{X} + \underline{Y}, \overline{X} + \overline{Y}\right]$
- $\begin{aligned} X - Y &= X + (-Y) \\ &= X + \left[-\overline{Y}, -\underline{Y}\right] = \left[\underline{X} - \overline{Y}, \overline{X} - \underline{Y}\right] \end{aligned}$
- $X.Y = [\min S, \max S]$ where $S = \underline{X}\underline{Y}, \underline{X}\overline{Y}, \overline{X}\underline{Y}, \overline{X}\overline{Y}$
- $X/Y = X.(1/Y)$
  where $1/Y = \{y : 1/y \in Y\} = \left[1/\overline{Y}, 1/\underline{Y}\right]; 0 \notin Y$.

Property B.3 (*Inclusion Isotonicity of Interval Arithmetic*). Let $\odot$ stand for addition, subtraction, multiplication, or division. Then, if A, B, C and D are intervals such that, $A \subseteq C$ and $B \subseteq D$, then

$$A \odot B \subseteq C \odot D$$

Given a real function f of real variables $x = [x_1, x_2, \dots, x_n]^T$ belonging to intervals $X = \left[X_1, X_2, \dots, X_n\right]^T$:

Definition B.3. The *interval extension function* (IEF), $F(X)$, is any interval-valued function that satisfies $F(x_1, x_2 \dots x_n) = f(x_1, x_2 \dots x_n)$. For degenerate interval arguments, the result must be the degenerate interval $\left[f(x_1, x_2 \dots x_n), f(x_1, x_2 \dots x_n)\right]$.

Definition B.4. We say that is $F = F(X_1, X_2, \dots .X_n)$ *inclusion isotonic* if

$$Y_i \subseteq X_i \forall i = 1, 2..n \Rightarrow F(Y_1, Y_2..Y_n) \subseteq F(X_1, X_2 \dots X_n)$$

An IEF which is *inclusion isotonic* guarantees the exact range containment.

Lemma B.4. *All rational interval functions are inclusion isotonic. Involving only interval arithmetic operators, which are inclusion isotonic, from the transitivity of partially ordered relation* $\subseteq$ *, it follows that they are always inclusion isotonic.*

Theorem B.1 (*Fundamental Theorem of Interval Analysis*). *If* F *is an inclusion isotonic interval extension of* f *, then* $f(X_1, X_2 \dots X_n) \subseteq F(X_1, X_2 \dots X_n)$.

The corresponding *rational interval function* can be found from *Natural interval extension* by expressing it as finite sequence of interval arithmetic operations as code list. As such, a RIF is inclusion isotonic and following result is obtained.

Corollary B.1. *If* F *is a rational interval function and an interval extension function of* f *, then* $f(X_1, X_2 \dots X_n) \subseteq F(X_1, X_2 \dots X_n)$.

Appendix C. Code list for URIFs evaluation

I-ARR 1:

$$T_{1,1} = sign(P_T).\left[\underline{\sqrt{|P_T - \Delta_{P_{T,u}}|}}, \overline{\sqrt{|P_T + \Delta_{P_{T,l}}|}}\right]; T_{1,2} = -\left[0, Cd_{T,2}\right]$$
$$T_1 = T_{1,1} * T_{1,2}$$
$$T_{2,1} = -\left[\underline{\delta_{A_T}}, \overline{\delta_{A_T}}\right].\frac{A_{T,n}}{\rho_T g}.\frac{dP_T}{dt}; T_2 = T_{2,1} + T_1$$
$$T_{3,1} = \frac{\left[-\Delta P_{T,l} - \Delta P_{T,u}, \Delta P_{T,l} + \Delta P_{T,u}\right]}{\Delta t}; T_{3,2} = -\left[\underline{A_T}, \overline{A_T}\right].(1/\rho_T g).T_{3,1}$$
$$T_3 = T_{3,2} + T_2;$$
$$T_4 = -\frac{1}{2} sign(P_T) Cd_{T,n}\left(\overline{\sqrt{|P_T + \Delta_{P_{T,l}}|}} - \underline{\sqrt{|P_T - \Delta_{P_{T,u}}|}}\right)[-1, 1]$$
$$\left[\underline{B_1}, \overline{B_1}\right] = T_1 + T_2 + T_3 + T_4$$

I-ARR 2:

$$U_{1,1} = -\frac{k_{2,n}}{k_{1,n}} * \left[\underline{\delta_{k_2}}, \overline{\delta_{k_2}}\right]; U_{1,2} = \left[\frac{\dot{m}_{22}}{b_1 k_{1,n}} - \frac{k_{2,n}}{k_{1,n}}, \frac{\dot{m}_{22}}{b_1 k_{1,n}} - \frac{k_{2,n}}{k_{1,n}}\right] + U_{1,1};$$
$$U_1 = -.\left[\underline{\delta_{1/k_1}}, \overline{\delta_{1/k_1}}\right] * U_{1,2}$$
$$U_{2,1} = -2.R_{z1,n}.F_1^2 * \left[\underline{\delta_{R_{z1}}}, \overline{\delta_{R_{z1}}}\right]; U_2 = U_{2,1} + U_1$$
$$U_{3,1} = \frac{k_{2,n}}{k_{1,n}} * \left[\underline{\delta_{k_2}}, \overline{\delta_{k_2}}\right]; U_3 = U_{3,1} + U_2$$
$$U_4 = -\left[-\Delta_{P_{T,l}}, -\Delta_{P_{T,u}}\right] + \left[-\Delta_{P_{B,l}}, -\Delta_{P_{B,u}}\right]$$
$$[\underline{B_2}, \overline{B_2}] = U_3 + U_4$$

I-ARR 3

$$V_{1,1} = sign(P_B).\left[\underline{\sqrt{|P_B - \Delta_{P_{B,u}}|}}, \overline{\sqrt{|P_B + \Delta_{P_{B,l}}|}}\right]; V_1 = -\left[0, Cd_{B,2}\right] * V_{1,1}$$
$$V_{2,1} = -\left[\underline{\delta_{1,C_B}}, \overline{\delta_{1,C_B}}\right].\frac{d\left(\rho_{l,n}(P_B).V_{l,n} + \rho_{v,n}(P_B).V_{v,n}\right)}{dt}; V_2 = V_{2,1} + V_1$$
$$V_3 = -\frac{1}{2} sign(P_B) Cd_{B,n}\left(\overline{\sqrt{|P_B + \Delta_{P_{B,l}}|}} - \underline{\sqrt{|P_B - \Delta_{P_{B,u}}|}}\right) * [-1, 1];$$
$$\left[\underline{B_3}, \overline{B_3}\right] = V_2 + V_3$$

I-ARR 4

$$W_1 = \left[\underline{\delta_{c_p}}, \overline{\delta_{c_p}}\right] c_{p,n}.T_2.F_1;$$
$$W_2 = b_2.\left[\underline{\delta_{1/RS}}, \overline{\delta_{1/RS}}\right]\frac{U_{in}^2}{RS_n} + W_1;$$
$$W_3 = -\left[\underline{\delta_{2,C_B}}, \overline{\delta_{2,C_B}}\right]\frac{d\left(\rho_{l,n}(P_B).V_{l,n}.h_{l,n}(P_B) + \rho_{v,n}(P_B).V_{v,n}.h_{v,n}(P_B)\right)}{dt} + W_2;$$
$$W_4 = -\left[\underline{\delta_{c_v}}, \overline{\delta_{c_v}}\right].c_{v_n}.T_6.F + W_3;$$
$$W_5 = -\left[\underline{\delta_{1/R_a}}, \overline{\delta_{1/R_a}}\right](1/R_{an}).(T_5 - T_a) + W_4$$
$$[\underline{B_4}, \overline{B_4}] = W_5$$

References

Benmoussa, S., Bouamama, B. O., & Merzouki, R. (2014). Bond graph approach for plant fault detection and isolation: Application to intelligent autonomous vehicle. *IEEE Transactions on Automation Science and Engineering*, *11*, 585–593.

Borutzky, W. (2011). *Bond graph modelling of engineering systems*. Springer.

Bouamama, B. O., Samantaray, A. K., Medjaher, K., Staroswiecki, M., & Dauphin-Tanguy, G. (2005). Model builder using functional and bond graph tools for FDI design. *Control Engineering Practice*, *13*, 875–891.

Bouamama, B. O., Samantaray, A., Staroswiecki, M., & Dauphin-Tanguy, G. (2003). Derivation of constraint relations from bond graph models for fault detection and isolation. *Simulation Series*, *35*, 104–109.

Bouamama, B. O., Staroswiecki, M., Riera, B., & Cherifi, E. (2000). Multi-modelling of an industrial steam generator. *Control Engineering Practice*, *8*, 1249–1260.

Chen, J., & Patton, R. J. (2012). *Robust model-based fault diagnosis for dynamic systems*. Springer Publishing Company, Incorporated.

Dauphin-Tanguy, G., & Kam, C. S. (1999). How to model parameter uncertainties in a bond graph framework. In *simulation in industry, 11th European simulation symposium* (pp. 121–125).

Djeziri, M. A., Merzouki, R., & Bouamama, B. O. (2009). Robust monitoring of an electric vehicle with structured and unstructured uncertainties. *IEEE Transactions on Vehicular Technology*, *58*, 4710–4719.

Djeziri, M. A., Merzouki, R., Bouamama, B. O., & Dauphin-Tanguy, G. (2007). Robust fault diagnosis by using bond graph approach. *IEEE/ASME Transactions on Mechatronics*, *12*, 599–611.

Djeziri, M. A., Ould Bouamama, B., & Merzouki, R. (2009). Modelling and robust <i>FDI </i>of steam generator using uncertain bond graph model. *Journal of Process Control*, *19*, 149–162.

El Harabi, R., Ould-Bouamama, B., Gayed, M. K. B., & Abdelkrim, M. N. (2010). Pseudo bond graph for fault detection and isolation of an industrial chemical reactor part I: bond graph modeling. In *Proceedings of the 2010 spring simulation multiconference* (p. 220). Society for Computer Simulation International.

Gertler, J. (1997). Fault detection and isolation using parity relations. *Control Engineering Practice*, *5*, 653–661.

Hansen, E., & Walster, G. W. (2003). *Global optimization using interval analysis: revised and expanded*. CRC Press.

Isermann, R. (2005). Model-based fault-detection and diagnosis–status and applications. *Annual Reviews in Control*, *29*, 71–85.

Jaulin, L., & Walter, E. (1993). Set inversion via interval analysis for nonlinear bounded-error estimation. *Automatica*, *29*, 1053–1064.

Jha, M., Dauphin-Tanguy, G., & Ould Bouamama, B. (2014a). Integrated diagnosis and prognosis of uncertain systems : A bond graph approach. In *Second European conference of the PHM society 2014 -Nantes France: European conference of the PHM society 2014 proceedings* (pp. 391–400).

Jha, M., Dauphin-Tanguy, G., & Ould Bouamama, B. (2014b). Robust FDI based on LFT BG and relative activity at junction. In *Control conference, ECC, 2014 European* (pp. 938–943). IEEE.

Karim, J., Jauberthie, C., & Combacau, M. (2008). Model-based fault detection method using interval analysis: Application to an aeronautic test bench. In *19th international workshop on principles of diagnosis DX* (pp. 269–273).

Karnopp, D. C., Margolis, D. L., & Rosenberg, R. C. (2012). *System dynamics: Modeling, simulation, and control of mechatronic systems*. Wiley.

Loureiro, R., Benmoussa, S., Touati, Y., Merzouki, R., & Ould Bouamama, B. (2014). Integration of fault diagnosis and fault-tolerant control for health monitoring of a class of MIMO intelligent autonomous vehicles. *IEEE Transactions on Vehicular Technology*, *63*, 30–39.

Medjaher, K., Samantaray, A. K., Ould Bouamama, B., & Staroswiecki, M. (2006). Supervision of an industrial steam generator. Part II: Online implementation. *Control Engineering Practice*, *14*, 85–96.

Moore, R. E. (1979). *Methods and applications of interval analysis*. SIAM.

Moore, R. E., Kearfott, R. B., & Cloud, M. J. (2009). *Introduction to interval analysis*. SIAM.

Mukherjee, A., & Samantaray, A. (2005). *SYMBOLS Shakti user's manual*. Kharagpur, India: High-Tech Consultants, STEP, Indian Institute of Technology.

Mukherjee, A., & Samantaray, A. K. (2006). *Bond graph in modeling, simulation and fault identification*. IK International Pvt Ltd.

Niu, G., Zhao, Y., Defoort, M., & Pecht, M. (2014). Fault diagnosis of locomotive electro-pneumatic brake through uncertain bond graph modeling and robust online monitoring. *Mechanical Systems and Signal Processing*.

Ould-Bouamama, B., El Harabi, R., Abdelkrim, M. N., & Ben Gayed, M. (2012). Bond graphs for the diagnosis of chemical processes. *Computers & Chemical Engineering*, *36*, 301–324.

Ould Bouamama, B., Medjaher, K., Bayart, M., Samantaray, A. K., & Conrard, B. (2005). Fault detection and isolation of smart actuators using bond graphs and external models. *Control Engineering Practice*, *13*, 159–175.

Ould Bouamama, B., Medjaher, K., Samantaray, A. K., & Staroswiecki, M. (2006). Supervision of an industrial steam generator. Part I: Bond graph modelling. *Control Engineering Practice*, *14*, 71–83.

Rinner, B., & Weiss, U. (2004). Online monitoring by dynamically refining imprecise models. *IEEE Transactions on Systems, Man and Cybernetics, Part B (Cybernetics)*, *34*, 1811–1822.

Rosenberg, R. C., & Karnopp, D. (1972). A definition of the bond graph language. *Journal of Dynamic Systems, Measurement, and Control*, *94*, 179–182.

Rump, S. M. (1999). *INTLAB—Interval laboratory*. Springer.

Samantaray, A. K., & Bouamama, B. O. (2008). *Model-based process supervision*. Springer.

Samantaray, A. K., Medjaher, K., Ould Bouamama, B., Staroswiecki, M., & Dauphin-Tanguy, G. (2006). Diagnostic bond graphs for online fault detection and isolation. *Simulation Modelling Practice and Theory*, *14*, 237–262.

Sié Kam, C., & Dauphin-Tanguy, G. (2005). Bond graph models of structured parameter uncertainties. *Journal of the Franklin Institute*, *342*, 379–399.

Staroswiecki, M., & Comtet-Varga, G. (2001). Analytical redundancy relations for fault detection and isolation in algebraic dynamic systems. *Automatica*, *37*, 687–699.

Thoma, J., & Bouamama, B. O. (2000). *Modelling and simulation in thermal and chemical engineering: A bond graph approach*. Springer.

Touati, Y., Merzouki, R., & Ould Bouamama, B. (2012). Robust diagnosis to measurement uncertainties using bond graph approach: Application to intelligent autonomous vehicle. *Mechatronics*, *22*, 1148–1160.

Further reading

Bouamama, B. O., Biswas, G., Loureiro, R., & Merzouki, R. (2014). Graphical methods for diagnosis of dynamic systems: Review. *Annual Reviews in Control*, *38*, 199–219.